International Journal of Control, Automation and Systems 18(2) (2020) 462-476
http://dx.doi.org/10.1007/s12555-018-0676-7
ISSN:1598-6446 eISSN:2005-4092
http://www.springer.com/12555

Fixed-time Synchronization of Complex-valued Memristive BAM Neural Network and Applications in Image Encryption and Decryption

Yongzhen Guo, Yang Luo*, Weiping Wang*, Xiong Luo, Chao Ge, Jürgen Kurths, Manman Yuan, and Yang Gao

Abstract: This paper focuses on the dynamical characteristics of complex-valued memristor-based BAM neural network (CVMBAMNN) with leakage time-varying delay. With two different controllers, we have obtained fixed-time and finite-time synchronization criteria respectively in complex domain for our special model, which few work has studied before. Since fixed-time synchronous system can improve communication security, we designed a scheme for RGB image encryption and decryption. In order to satisfy the requirement of much lower error in image secure communication, our approach can get the error of fixed-time synchronization to about 1×10^{-13}. Due to our highly consistent system, we do get good encryption and decryption effect with encryption and decryption scheme. Finally, numerical simulations are included to demonstrate the correctness of our theoretical results.

Keywords: Chaotic character, complex-valued MBAMNN, fixed-time synchronization, image encryption and decryption, leakage time-varying delay.

1. INTRODUCTION

Bidirectional associative memories neural network (BAMNN) is a two-layer nonlinear feedback network, which has been proposed by Kosok in 1987 [1]. In recent years, BAM has been applied to many fields. For instance, authors in [2] used BAMNN model to achieve application to inverter's fault diagnosis. In [3], authors applied BAMNN to industrial spectral signatures. Memristor-based BAMNN (MABMNN) [4] is a kind of BAM neural networks, connection weights of which are replaced by memristor due to that the memristor can be better simulate the function of synapse. However, more studies on MBAMNN are only in real domain. Since Fourier proposed Fourier transform, signals are mapped to frequency domain and complex domain with the method of Fourier transform. Moreover, some problems cannot be solved in real number domain. For example, authors in [5] introduced that the symmetry problem and XOR problem could be solved by complex-valued neurons with the orthogonal decision boundaries, while real-valued neurons failed to do it.

Complex-valued neural network (CVNN) has become popular in recent years, since nonlinear systems in real number domains are not that fit with special issues or requirements of some engineering applications. CVNN [6–10], inputs/outputs, weights and activate functions of which are all in complex domain, is different from traditional neural network.

Like BAM neural network, complex-valued MBAM neural network (CVMBAMNN) is also a kind of chaotic system. CVMBAMNN is different from MBAMNN on that its parameters are separated into two parts: the real part and the imaginary part, and the state of every neu-

Manuscript received September 20, 2018; revised February 21, 2019, February 23, 2019, and June 28, 2019; accepted July 3, 2019. Recommended by Associate Editor Ohmin Kwon under the direction of Editor Euntai Kim. This work was supported in part by the National Key Research and Development Program of China under Grant 2016YFB0800205, and the National Key Research and Development Program of China under Grant No. 2018YFB0803505, and the National Natural Science Foundation of China under Grants U1836106, the Fundamental Research Funds for the Central Universities FRF-TP-19-005A3, the National Nature Science Foundation of China under Grant U1836106, and the University of Science and Technology Beijing-National Taipei University of Technology Joint Research Program under Grant TW201705.

Yongzhen Guo is with the School of Automation,Beijing Institute of Technology(BIT),China, and China Software Testing Center, China (e-mail: yzguo@cstc.org.cn). Yang Luo is with the School of Automation and Electrical Engineering, University of Science and Technology Beijing (USTB), Beijing 100083, China (e-mail: m18811355098@163.com). Weiping Wang and Manman Yuan are with the School of Computer and Communication Engineering, University of Science and Technology Beijing (USTB), Beijing 100083, China, Beijing Key Laboratory of Knowledge Engineering for Materials Science, Beijing 100083, China, and Institute of Physics, Humboldt-University, Berlin 10099, Germany (e-mails: weipingwangjt@ustb.edu.cn, yuanman_an_smile@163.com). Xiong Luo is with the School of Computer and Communication Engineering, University of Science and Technology Beijing (USTB), Beijing 100083, China (e-mail: xluo@ustb.edu.cn). Chao Ge is with the Institute of Information Engineering, North China University of Science and Technology, Tangshan 063210, China (e-mail: gechao365@126.com). Jürgen Kurths is with the Institute of Physics, Humboldt-University Berlin, 10099 Berlin, Germany, and Potsdam Institute for Climate Impact Research, 14473 Potsdam, Germany (e-mail: kurths@pik-potsdam.de). Yang Gao is with China Information Technology Security Evaluation Center, China (e-mail: gaoy@itsec.gov.cn).
* Corresponding author.

ron is also in complex domain. Due to its randomness, ergodicity, certainty and sensitivity to initial conditions, in theory, chaotic system [11] may have infinite number of states with different initial conditions. In our views, there are few people to study the dynamic behaviors of CVMBAMNN, which encourages our idea.

In the human brain, the transmission of information is often accompanied by time delays that usually change with time and the state of neurons [12]. Found in the negative feedback term of system, leakage delay or forgetting delays [4] is one of the two time-varying delays, and another one is named distribute time delays. Authors in [13] illustrated that the time delay in the leakage term would have a tendency to destabilize a system. To increase model's conservation, it is necessary to consider leakage delay in the research of neural networks.

As one of the most important studies of neural networks, synchronization, which means that the dynamical behaviors of master and slave systems tend to be consistent, is a hot topic. Based on Lyapunov function and stability theory [14], synchronization studies can be divided into finite-time synchronization [15, 16] and fixed-time synchronization [17, 18]. Explained by authors in [17], the settling time T of finite-time synchronization depends on the initial synchronization errors of the system, which means that the initial conditions should be known beforehand. However, not all the initial values of the systems are available in practice. Due to finite-time synchronization's weakness above, scholars proposed fixed-time synchronization, and sufficient conditions of the fixed-time synchronization of nonlinear systems were first given by Polyakov [19]. The maximum stable time of fixed-time synchronization just depends on the parameters of controllers. Absent from the study, the main work of this paper is the fixed-time synchronization of the CVMBAMNN with leakage time-varying delays.

Since image secure communication [20, 21] is an important component in industrial applications, how to build a strong encryption and decryption model is the key point. Due to the complex dynamic behavior of neural networks, more and more researches apply such character into image encryption and decryption. Traditional image encryption algorithm can be easily decrypted due to its insufficient complexity. Instead, with chaotic characters, chaotic encryption [22, 23] has become increasingly popular due to its advantages of simplicity, efficiency and safety. Combining the chaotic character, image encryption and decryption are considered as an application, according to our CVMBAMNN, which are rare.

The remaining chapters of this paper are arranged as follows: 1) In Section 2, including its drive, response and error systems, model of CVMBAMNN is constructed. Some preliminaries are proposed in this section. 2) In Section 3, we give the proof of fixed-time synchronization of CVMBAMNN with leakage time-varying delay. 3) In Section 4, simulations are designed to demonstrate our theory above. Applications in image encryption and decryption are shown. 4) Finally, conclusions of the obtained results in this paper are given in Section 5.

2. PRELIMINARIES

In this paper, the solutions of all the systems are based on Filippov's sense. R^n and C^n denote n-dimensional Euclidean space and complex space. For complex-valued function $z^u = z^R + iz^I \in \mathrm{C}$, i is the imaginary unit and satisfies $i^2 = -1$. Consider the following MBAMNN model with leakage time-varying delay with complex values(CVMBAMNN):

$$\begin{cases} \dot{z}^u_{1i}(t) = -\delta^u_i(z^u_{1i}(t-\tau(t)))z^u_{1i}(t-\tau(t)) \\ \qquad\quad + \sum_{j=1}^{m} a^u_{ji}(z^u_{1i}(t))f^u_j(z^u_{2j}(t)) \\ \qquad\quad + \sum_{j=1}^{m} b^u_{ji}(z^u_{1i}(t-\tau(t)))f^u_j(z^u_{2j}(t-\sigma(t))), \\ \dot{z}^u_{2j}(t) = -\rho^u_j(z^u_{2j}(t-\sigma(t)))z^u_{2j}(t-\sigma(t)) \\ \qquad\quad + \sum_{i=1}^{n} c^u_{ij}(z^u_{2j}(t))g^u_i(z^u_{1i}(t)) \\ \qquad\quad + \sum_{i=1}^{n} d^u_{ij}(z^u_{2j}(t-\sigma(t)))g^u_i(z^u_{1i}(t-\tau(t))), \end{cases} \tag{1}$$

where $z^u_{1i}(t)$ and $z^u_{2j}(t)$ are complex-valued state vectors of the ith and jth neuron, respectively, for $i = 1, 2, ..., m$, $j = 1, 2, ..., n$. Let $z^u_{1i}(t) = (z^u_{11}(t), z^u_{12}(t),..., z^u_{1m}(t))^T$, and $z^u_{2j}(t) = (z^u_{21}(t), z^u_{22}(t), ..., z^u_{2n}(t))^T$, $u = R, I$. The initial values of system (1) are $z^u_1(0) = \varphi 1^u(s)$ and $z^u_2(0) = \varphi 2^u(s)$. $\delta^u_i > 0$ and $\rho^u_j > 0$ are the rates of neuron self-inhibition, and their values depend on the state of neuron with leakage time-varying delay; $f^u_j(\cdot)$ and $g^u_i(\cdot)$ are the activation functions; $\tau(t)$ and $\sigma(t)$ are the time-varying delays, which satisfy $C1 < \tau(t), C2 < \sigma(t)$, $\dot{\tau}(t) \le C3$ and $\dot{\sigma}(t) \le C4$ ($C1$, $C2$, $C3$ and $C4$ are constants). This paper only discusses the case where the delays are continuous. a^u_{ji}, b^u_{ji}, c^u_{ij}, d^u_{ij} are the memristive connection weights, and their values also depend on the states of neurons.

Based on the properties of memristor, we set:

$$\delta^R_i(z) = \begin{cases} \check{\delta}^R_i, & |z| \ge T_i, \\ \hat{\delta}^R_i, & |z| < T_i, \end{cases} \quad \delta^I_i(z) = \begin{cases} \check{\delta}^I_i, & |z| \ge T_i, \\ \hat{\delta}^I_i, & |z| < T_i, \end{cases}$$

$$\rho^R_j(z) = \begin{cases} \check{\rho}^R_j, & |z| \ge T'_j, \\ \hat{\rho}^R_j, & |z| < T'_j, \end{cases} \quad \rho^I_j(z) = \begin{cases} \check{\rho}^I_j, & |z| \ge T'_j, \\ \hat{\rho}^I_j, & |z| < T'_j, \end{cases}$$

$$a^R_{ji}(z) = \begin{cases} \check{A}^R_{ji}, & |z| \ge \Delta_i, \\ \hat{A}^{*R}_{ji}, & |z| < \Delta_i, \end{cases} \quad a^I_i(z) = \begin{cases} \check{A}^I_i, & |z| \ge \Delta_i, \\ \hat{A}^{*I}_i, & |z| < \Delta_i, \end{cases}$$

$$b^R_{ji}(z) = \begin{cases} \check{B}^R_{ji}, & |z| \ge \Delta'_i, \\ \hat{B}^{*R}_{ji}, & |z| < \Delta'_i, \end{cases} \quad b^I_{ji}(z) = \begin{cases} \check{B}^I_i, & |z| \ge \Delta'_i, \\ \hat{B}^{*I}_i, & |z| < \Delta'_i, \end{cases}$$

$$c_{ij}^R(z)=\begin{cases}\check{C}_{ij}^R, & |z|\geq\Lambda_j,\\ \hat{C}_{ij}^{*R}, & |z|<\Lambda_j,\end{cases}\quad c_{ij}^I(z)=\begin{cases}\check{C}_j^I, & |z|\geq\Lambda_j,\\ \hat{C}_j^{*I}, & |z|<\Lambda_j,\end{cases}$$

$$d_{ij}^R(z)=\begin{cases}\check{D}_{ij}^R, & |z|\geq\Lambda_j',\\ \hat{D}_{ij}^{*R}, & |z|<\Lambda_j',\end{cases}\quad d_{ij}^I(z)=\begin{cases}\check{D}_j^I, & |z|\geq\Lambda_j',\\ \hat{D}_j^{*I}, & |z|<\Lambda_j'.\end{cases}$$

Here $\left|\acute{\delta}_i^{R+}\right|=\max\left\{\left|\check{\delta}_i^R\right|,\ \left|\hat{\delta}_i^R\right|\right\}$, $\left|\acute{\delta}_i^{I+}\right|=\max\left\{\left|\check{\delta}_i^I\right|,\ \left|\hat{\delta}_i^I\right|\right\}$, $\left|\acute{\rho}_j^{R+}\right|=\max\left\{\left|\check{\rho}_j^R\right|,\ \left|\hat{\rho}_j^R\right|\right\}$, $\left|\acute{\rho}_j^{I+}\right|=\max\left\{\left|\check{\rho}_j^I\right|,\ \left|\hat{\rho}_j^I\right|\right\}$.

Considering system (1) as the drive systems, the corresponding response systems can be described as follows:

$$\begin{cases}\dot{\tilde{z}}_{1i}^u(t)=-\delta_i^u(\tilde{z}_{1i}^u(t-\tau(t)))\tilde{z}_{1i}^u(t-\tau(t))\\ \qquad+\sum_{j=1}^m a_{ji}^u(\tilde{z}_{1i}^u(t))f_j^u(\tilde{z}_{2j}^u(t))\\ \qquad+\sum_{j=1}^m b_{ji}^u(\tilde{z}_{1i}^u(t-\tau(t)))f_j^u(\tilde{z}_{2j}^u(t-\sigma(t)))\\ \qquad+u_i^u(t),\\ \dot{\tilde{z}}_{2j}^u(t)=-\rho_j^u(\tilde{z}_{2j}^u(t-\sigma(t)))\tilde{z}_{2j}^u(t-\sigma(t))\\ \qquad+\sum_{i=1}^n c_{ij}^u(\tilde{z}_{2j}^u(t))g_i^u(\tilde{z}_{1i}^u(t))\\ \qquad+\sum_{i=1}^n d_{ij}^u(\tilde{z}_{2j}^u(t-\sigma(t)))g_i^u(\tilde{z}_{1i}^u(t-\tau(t)))\\ \qquad+v_j^u(t),\end{cases}\tag{2}$$

$i=1,\ 2,\ ...,\ m,\ j=1,\ 2,\ ...,\ n$, where $u_i(t)$ and $v_j(t)$ are the appropriate feedback controllers. Let $\tilde{z}_{1i}^u(t)=(\tilde{z}_{11}^u(t),\ \tilde{z}_{12}^u(t),\ ...,\ \tilde{z}_{1m}^u(t))^T$, and $\tilde{z}_{2j}^u(t)=(\tilde{z}_{21}^u(t),\tilde{z}_{22}^u(t),\ ...,\ \tilde{z}_{2n}^u(t))^T$, the initial values of response system (2) are $\tilde{z}_1^u(0)=\tilde{\varphi}1^u(s)$ and $\tilde{z}_2^u(0)=\tilde{\varphi}2^u(s)$.

Remark 1: Saturation limit is a kind of common actuator nonlinearities in practical control systems. When controller meets input limit, the value of output would not change [24]. Though our system is an interest nonlinear one due to its hyper chaotic character, in this paper, we would not discuss such saturation limit. But it deserves to be our future research direction.

According to system (1) and (2), here we define synchronization errors as $e_{1i}^R(t)=\tilde{z}_{1i}^R(t)-z_{1i}^R(t)$, $e_{1i}^I(t)=\tilde{z}_{1i}^I(t)-z_{1i}^I(t)$, $i=1,\ 2,\ ...,\ m$, $e_{2j}^R(t)=\tilde{z}_{2j}^R(t)-z_{2j}^R(t)$, $e_{2j}^I(t)=\tilde{z}_{2j}^I(t)-z_{2j}^I(t)$, $j=1,2,...,n$. The error system is defined as follows:

$$\begin{cases}\dot{e}_{1i}^R(t)=-\Big[\delta_i^R(\tilde{z}_{1i}^R(t-\tau(t)))\tilde{z}_{1i}^R(t-\tau(t))\\ \qquad-\delta_i^I(\tilde{z}_{1i}^I(t-\tau(t)))\tilde{z}_{1i}^I(t-\tau(t))\Big]\\ \qquad+\Big[\delta_i^R(z_{1i}^R(t-\tau(t)))z_{1i}^R(t-\tau(t))\\ \qquad-\delta_i^I(z_{1i}^I(t-\tau(t)))z_{1i}^I(t-\tau(t))\Big]\\ \qquad+F_i^R(t)+u_i^R(t),\\ \dot{e}_{1i}^I(t)=-\Big[\delta_i^R(\tilde{z}_{1i}^R(t-\tau(t)))\tilde{z}_{1i}^I(t-\tau(t))\\ \qquad-\delta_i^I(\tilde{z}_{1i}^I(t-\tau(t)))\tilde{z}_{1i}^R(t-\tau(t))\Big]\\ \qquad+\Big[\delta_i^R(z_{1i}^R(t-\tau(t)))z_{1i}^I(t-\tau(t))\\ \qquad+\delta_i^I(z_{1i}^I(t-\tau(t)))z_{1i}^R(t-\tau(t))\Big]\\ \qquad+F_i^I(t)+u_i^I(t),\\ \dot{e}_{2j}^R(t)=-\Big[\rho_j^R(\tilde{z}_{2j}^R(t-\sigma(t)))\tilde{z}_{2j}^R(t-\sigma(t))\\ \qquad-\rho_j^I(\tilde{z}_{2j}^I(t-\sigma(t)))\tilde{z}_{2j}^I(t-\sigma(t))\Big]\\ \qquad+\Big[\rho_j^R(z_{2j}^R(t-\sigma(t)))z_{2j}^R(t-\sigma(t))\\ \qquad-\rho_j^I(z_{2j}^I(t-\sigma(t)))z_{2j}^I(t-\sigma(t))\Big]\\ \qquad+G_j^R(t)+v_j^R(t),\\ \dot{e}_{2j}^I(t)=-\Big[\rho_j^I(\tilde{z}_{2j}^I(t-\sigma(t)))\tilde{z}_{2j}^R(t-\sigma(t))\\ \qquad+\rho_j^R(\tilde{z}_{2j}^R(t-\sigma(t)))\tilde{z}_{2j}^I(t-\sigma(t))\Big]\\ \qquad+\Big[\rho_j^I(z_{2j}^I(t-\sigma(t)))z_{2j}^R(t-\sigma(t))\\ \qquad+\rho_j^R(z_{2j}^R(t-\sigma(t)))z_{2j}^I(t-\sigma(t))\Big]\\ \qquad+G_j^I(t)+v_j^I(t),\end{cases}\tag{3}$$

for $i=1,\ 2,\ ...,\ n,\ j=1,\ 2,\ ...,\ m$, where we define $F_i^R(t),F_i^I(t),G_j^R(t),G_j^I(t)$ as follows:

$$\begin{aligned}F_i^R(t)=&\sum_{j=1}^m\Big\{a_{ji}^R(\tilde{z}_{1i}^R(t))f_j^R(\tilde{z}_{2j}^R(t))-a_{ji}^R(z_{1i}^R(t))f_j^R(z_{2j}^R(t))\\ &+a_{ji}^I(z_{1i}^I(t))f_j^I(z_{2j}^I(t))-a_{ji}^I(\tilde{z}_{1i}^I(t))f_j^I(\tilde{z}_{2j}^I(t))\Big\}\\ &+\sum_{j=1}^m\Big\{b_{ji}^R(\tilde{z}_{1i}^R(t-\tau(t)))f_j^R(\tilde{z}_{2j}^R(t-\sigma(t)))\\ &-b_{ji}^R(z_{1i}^R(t-\tau(t)))f_j^R(z_{2j}^R(t-\sigma(t)))\Big\}\\ &+\sum_{j=1}^m\Big\{b_{ji}^I(z_{1i}^I(t-\tau(t)))f_j^I(z_{2j}^I(t-\sigma(t)))\\ &-b_{ji}^I(\tilde{z}_{1i}^I(t-\tau(t)))f_j^I(\tilde{z}_{2j}^I(t-\sigma(t)))\Big\},\end{aligned}\tag{4}$$

$$\begin{aligned}F_i^I(t)=&\sum_{j=1}^m\Big\{a_{ji}^I(\tilde{z}_{1i}^I(t))f_j^R(\tilde{z}_{2j}^R(t))-a_{ji}^I(z_{1i}^I(t))f_j^R(z_{2j}^R(t))\\ &+a_{ji}^R(\tilde{z}_{1i}^R(t))f_j^I(\tilde{z}_{2j}^I(t))-a_{ji}^R(z_{1i}^R(t))f_j^I(z_{2j}^I(t))\Big\}\\ &+\sum_{j=1}^m\Big\{b_{ji}^R(\tilde{z}_{1i}^R(t-\tau(t)))f_j^I(\tilde{z}_{2j}^I(t-\sigma(t)))\\ &-b_{ji}^R(z_{1i}^R(t-\tau(t)))f_j^I(z_{2j}^I(t-\sigma(t)))\Big\}\\ &+\sum_{j=1}^m\Big\{b_{ji}^I(\tilde{z}_{1i}^I(t-\tau(t)))f_j^R(\tilde{z}_{2j}^R(t-\sigma(t)))\\ &-b_{ji}^I(z_{1i}^I(t-\tau(t)))f_j^R(z_{2j}^R(t-\sigma(t)))\Big\},\end{aligned}\tag{5}$$

$$G_j^R(t)=\sum_{i=1}^{n}\Big\{c_{ij}^R(\tilde{z}_{2j}^R(t))g_i^R(\tilde{z}_{1i}^R(t))-c_{ij}^R(z_{2j}^R(t))g_i^R(z_{1i}^R(t))$$
$$+c_{ij}^I(z_{2j}^I(t))g_i^I(z_{1i}^I(t))-c_{ij}^I(\tilde{z}_{2j}^I(t))g_i^I(\tilde{z}_{1i}^I(t))\Big\}$$
$$+\sum_{i=1}^{n}\Big\{d_{ij}^R(\tilde{z}_{2j}^R(t-\sigma(t)))g_i^R(\tilde{z}_{1i}^R(t-\tau(t)))$$
$$-d_{ij}^R(z_{2j}^R(t-\sigma(t)))g_i^I(z_{1i}^I(t-\tau(t)))\Big\}$$
$$+\sum_{i=1}^{n}\Big\{d_{ij}^R(\tilde{z}_{2j}^R(t-\sigma(t)))g_i^R(\tilde{z}_{1i}^R(t-\tau(t)))$$
$$-d_{ij}^I(z_{2j}^I(t-\sigma(t)))g_i^I(z_{1i}^I(t-\tau(t)))\Big\}, \quad (6)$$

$$G_j^I(t)=\sum_{i=1}^{n}\Big\{c_{ij}^I(\tilde{z}_{2j}^I(t))g_i^R(\tilde{z}_{1i}^R(t))-c_{ij}^I(z_{2j}^I(t))g_i^R(z_{1i}^R(t))$$
$$c_{ij}^R(\tilde{z}_{2j}^R(t))g_i^I(\tilde{z}_{1i}^I(t))-c_{ij}^I(z_{2j}^I(t))g_i^R(z_{1i}^R(t))\Big\}$$
$$+\sum_{i=1}^{n}\Big\{d_{ij}^R(\tilde{z}_{2j}^R(t-\sigma(t)))g_i^I(\tilde{z}_{1i}^I(t-\tau(t)))$$
$$-d_{ij}^R(z_{2j}^R(t-\sigma(t)))g_i^I(z_{1i}^I(t-\tau(t)))\Big\}$$
$$+\sum_{i=1}^{n}\Big\{d_{ij}^I(\tilde{z}_{2j}^I(t-\sigma(t)))g_i^R(\tilde{z}_{1i}^R(t-\tau(t)))$$
$$-d_{ij}^I(z_{2j}^I(t-\sigma(t)))g_i^R(z_{1i}^R(t-\tau(t)))\Big\}. \quad (7)$$

Let $e_{1i}^u(t)=(e_{11}^u(t),\ e_{12}^u(t),\ ...,\ e_{1n}^u(t))^T$, $e_{2j}^u(t)=(e_{21}^u(t),\ e_{22}^u(t),\ ...,\ e_{2m}^u(t))^T$, the initial values of error system (3) are $e_1^R(s)=\widetilde{\varphi}1^R(s)-\varphi 1^R(s)$, $e_1^I(s)=\widetilde{\varphi}1^I(s)-\varphi 1^I(s)$, $e_2^R(s)=\widetilde{\varphi}2^R(s)-\varphi 2^R(s)$, $e_2^I(s)=\widetilde{\varphi}2^I(s)-\varphi 2^I(s)$.

To obtain synchronization criteria, some assumptions and lemmas are made as follows:

Assumption 1: There exits constant $M_j^R>0$, so that $|f_j^R|\le M_j^R$, $j=1,\ ...,\ m$.

Assumption 2: There exits constant $M_j^I>0$, so that $|f_j^I|\le M_j^I$, $j=1,\ ...,\ m$.

Assumption 3: There exits constant $N_i^R>0$, so that $|g_i^R|\le N_i^R$,$i=1,\ ...,\ n$.

Assumption 4: There exits constant $N_i^I>0$, so that $|g_i^I|\le N_i^I$,$i=1,\ ...,\ n$.

Here we define:

$$|\acute{a}_{ji}^{R+}|=\max\{|\check{A}_{ji}^R|,|\hat{A}_{ji}^{*R}|\},\ \ |\acute{a}_{ji}^{I+}|=\max\{|\check{A}_{ji}^I|,|\hat{A}_{ji}^{*I}|\};$$
$$|\acute{b}_{ji}^{R+}|=\max\{|\check{B}_{ji}^R|,|\hat{B}_{ji}^{*R}|\},\ \ |\acute{b}_{ji}^{I+}|=\max\{|\check{B}_{ji}^I|,|\hat{B}_{ji}^{*I}|\};$$
$$|\acute{c}_{ij}^{R+}|=\max\{|\check{C}_{ij}^R|,|\hat{C}_{ij}^{*R}|\},\ \ |\acute{c}_{ij}^{I+}|=\max\{|\check{C}_{ij}^I|,|\hat{C}_{ij}^{*I}|\};$$
$$|\acute{d}_{ij}^{R+}|=\max\{|\check{D}_{ij}^R|,|\hat{D}_{ij}^{*R}|\},\ \ |\acute{d}_{ij}^{I+}|=\max\{|\check{D}_{ij}^I|,|\hat{D}_{ij}^{*I}|\}.$$

Lemma 1: $|F_i^R(t)|\le\chi_i^R$ for $\chi_i^R=2\sum_{j=1}^m[M_j^R(\acute{a}_{ji}^R+\acute{b}_{ji}^R)+M_j^I(\acute{a}_{ji}^I+\acute{b}_{ji}^I)]$, $j=1,2,...,m$.

Proof: With Assumption 1, it can be proved as follows:

$$F_i^R(t)\le\sum_{j=1}^{m}\Big\{a_{ji}^R(\tilde{z}_{1i}^R(t))M_j^R-a_{ji}^R(z_{1i}^R(t))M_j^R$$
$$+a_{ji}^I(z_{1i}^I(t))M_j^I-a_{ji}^I(\tilde{z}_{1i}^I(t))M_j^I\Big\}$$
$$+\sum_{j=1}^{m}\Big\{b_{ji}^R(\tilde{z}_{1i}^R(t-\tau(t)))$$
$$-b_{ji}^R(z_{1i}^R(t-\tau(t)))\Big\}M_j^R$$
$$+\sum_{j=1}^{m}\Big\{b_{ji}^I(z_{1i}^I(t-\tau(t)))$$
$$-b_{ji}^I(\tilde{z}_{1i}^I(t-\tau(t)))\Big\}M_j^I$$
$$\le\sum_{j=1}^{m}\Big\{|a_{ji}^R(\tilde{z}_{1i}^R(t))|+|a_{ji}^R(z_{1i}^R(t))|\Big\}M_j^R$$
$$+|a_{ji}^I(z_{1i}^I(t))|M_j^I+|a_{ji}^I(\tilde{z}_{1i}^I(t))|M_j^I\Big\}$$
$$+\sum_{j=1}^{m}\Big\{|b_{ji}^R(\tilde{z}_{1i}^R(t-\tau(t)))|$$
$$+|b_{ji}^R(z_{1i}^R(t-\tau(t)))\Big\}|M_j^R$$
$$+\sum_{j=1}^{m}\Big\{|b_{ji}^I(z_{1i}^I(t-\tau(t)))$$
$$+|b_{ji}^I(\tilde{z}_{1i}^I(t-\tau(t)))\Big\}|M_j^I.$$

In the end, we can prove that:

$$|F_i^R(t)|\le\chi_i^R$$

for $\chi_i^R=2\sum_{j=1}^m[M_j^R(\acute{a}_{ji}^{R+}+\acute{b}_{ji}^{R+})+M_j^I(\acute{a}_{ji}^{I+}+\acute{b}_{ji}^{I+})]$, $j=1,2,...,m$.

Lemma 2: 1) $|F_i^I(t)|\le\chi_i^I$ for $\chi_i^I=2\sum_{j=1}^m[M_j^R(\acute{a}_{ji}^{I+}+\acute{b}_{ji}^{I+})+M_j^I(\acute{a}_{ji}^{R+}+\acute{b}_{ji}^{R+})]$; 2) $|G_j^R(t)|\le\Omega_i^R$ for $\Omega_i^R=2\sum_{i=1}^n[N_i^R(\acute{c}_{ij}^{R+}+\acute{d}_{ij}^{R+})+N_i^I(\acute{c}_{ij}^{I+}+\acute{d}_{ij}^{I+})]$; 3) $|G_j^I(t)|\le\Omega_i^I$ for $\Omega_i^I=2\sum_{i=1}^n[N_i^R(\acute{c}_{ij}^{I+}+\acute{d}_{ij}^{I+})+N_i^I(\acute{c}_{ij}^{R+}+\acute{d}_{ij}^{R+})]$, for $i=1,2,...,n$, $j=1,2,...,m$. According to Assumptions 2, 3 and 4, proofs are similar with Lemma 1, so they are omitted here.

Lemma 3 [25]**:** We have:

$$\Big|-\Big[\delta_i^R(\tilde{z}_{1i}^R(t-\tau(t)))\tilde{z}_{1i}^R(t-\tau(t))$$
$$-\delta_i^I(\tilde{z}_{1i}^I(t-\tau(t)))\tilde{z}_{1i}^I(t-\tau(t))\Big]$$
$$+\Big[\delta_i^R(z_{1i}^R(t-\tau(t)))z_{1i}^R(t-\tau(t))$$
$$-\delta_i^I(z_{1i}^I(t-\tau(t)))z_{1i}^I(t-\tau(t))\Big]\Big|$$
$$\le\acute{\delta}_i^{R+}\Big|\tilde{z}_{1i}^R(t-\tau(t))-z_{1i}^R(t-\tau(t))\Big|$$
$$+\acute{\delta}_i^{I+}\Big|\tilde{z}_{1i}^I(t-\tau(t))-z_{1i}^I(t-\tau(t))\Big|, \quad (8)$$
$$\Big|-\Big[\delta_i^R(\tilde{z}_{1i}^R(t-\tau(t)))\tilde{z}_{1i}^I(t-\tau(t))$$
$$-\delta_i^I(\tilde{z}_{1i}^I(t-\tau(t)))\tilde{z}_{1i}^R(t-\tau(t))\Big]$$
$$+\Big[\delta_i^R(z_{1i}^R(t-\tau(t)))z_{1i}^I(t-\tau(t))$$
$$-\delta_i^I(z_{1i}^I(t-\tau(t)))z_{1i}^R(t-\tau(t))\Big]\Big|$$

$$\le \acute{\delta}_i^{R+}\left|\tilde{z}_{1i}^I(t-\tau(t))-z_{1i}^I(t-\tau(t))\right| + \acute{\delta}_i^{I+}\left|\tilde{z}_{1i}^R(t-\tau(t))-z_{1i}^R(t-\tau(t))\right|, \tag{9}$$

$$\begin{aligned}\Big|&-\Big[\rho_j^R(\tilde{z}_{2j}^R(t-\sigma(t)))\tilde{z}_{2j}^R(t-\sigma(t)) - \rho_j^I(\tilde{z}_{2j}^I(t-\sigma(t)))\tilde{z}_{2j}^I(t-\sigma(t))\Big] \\ &+\Big[\rho_j^R(z_{2j}^R(t-\sigma(t)))z_{2j}^R(t-\sigma(t)) - \rho_j^I(z_{2j}^I(t-\sigma(t)))z_{2j}^I(t-\sigma(t))\Big]\Big| \\ &\le \acute{\rho}_j^{R+}\left|\tilde{z}_{2j}^R(t-\sigma(t))-z_{2j}^R(t-\sigma(t))\right| + \acute{\rho}_i^{I+}\left|\tilde{z}_{2j}^I(t-\sigma(t))-z_{2j}^I(t-\sigma(t))\right|,\end{aligned} \tag{10}$$

$$\begin{aligned}\Big|&-\Big[\rho_j^I(\tilde{z}_{2j}^I(t-\sigma(t)))\tilde{z}_{2j}^R(t-\sigma(t)) + \rho_j^R(\tilde{z}_{2j}^R(t-\sigma(t)))\tilde{z}_{2j}^I(t-\sigma(t))\Big] \\ &+\Big[\rho_j^I(z_{2j}^I(t-\sigma(t)))z_{2j}^R(t-\sigma(t)) + \rho_j^R(z_{2j}^R(t-\sigma(t)))z_{2j}^I(t-\sigma(t))\Big]\Big| \\ &\le \acute{\rho}_j^{R+}\left|\tilde{z}_{2j}^I(t-\sigma(t))-z_{2j}^I(t-\sigma(t))\right| + \acute{\rho}_i^{I+}\left|\tilde{z}_i^R(t-\sigma(t))-z_{2j}^R(t-\sigma(t))\right|.\end{aligned} \tag{11}$$

Lemma 4 [26]**:** If $x_1, x_2, ..., x_n \ge 0$, $0 < p \le 1$, $q > 1$, then we have:

$$\sum_{i=1}^n x_i^p \ge (\sum_{i=1}^n x_i)^p, \quad \sum_{i=1}^n x_i^q \ge n^{1-q}(\sum_{i=1}^n x_i)^q. \tag{12}$$

Definition 1: System (2) is said to be synchronized with system (1) in finite time if there exists a constant t* and $|e(t)| \equiv 0$ when $\forall t \ge t*$. $e(t*) = (e_{11}^R(t), e_{12}^R(t), ..., e_{1m}^R(t), e_{11}^I(t), e_{12}^I(t), ..., e_{1m}^I(t), e_{21}^R(t), e_{22}^R(t), ..., e_{2n}^R(t), e_{21}^I(t), e_{22}^I(t), ..., e_{2n}^I(t))$. Besides, $t*$ is called as the setting time and e(t*) change with the differences of initial value.

Lemma 5 [27]**:** Suppose a nonnegative function $V(t)$ satisfies $\dot{V}(t) \le -\alpha V^p(t)$, $0 < p < 1$, where $\alpha > 0$. Then $V(t) \equiv 0$ for all $t \ge T_{max}$, where $T_{max} = \frac{V^{1-p}(0)}{\alpha(1-p)}$. Then system is finite-time stable.

Definition 2: System (1) and (2) are said to achieve fixed-time synchronization, if there exists a constant $t*$ and $|e(t)| \equiv 0$ when $\forall t \ge t*$. And no matter what values of $e(0)$ are, the response system's stable time $t* \le T_{max}$ for $T_{max} > 0$.

Lemma 6 [19]**:** Let $V(\cdot)$: $R_n \to R_+$ be a continuous radically unbounded function. Suppose the following two conditions hold:

1) $V(e) = 0 \Leftrightarrow e = 0$;

2) For a, $b > 0$, $0 < p < 1$ and $q > 1$, if $e(t)$ of error system (3) satisfies $\dot{V}(e(t)) \le -aV^p(e(t)) - bV^q(e(t))$, then the error system (3) is fixed-time stable, and $T_{max} = \frac{1}{a(1-p)} + \frac{1}{b(q-1)}$. What is more, $V(t)$ satisfies: $V(t) \equiv 0$, $t \ge T(e_0)$, and $T(e_0) \le T_{max}$.

3. MAIN RESULTS

In this subsection, we give the proof of achieving fixed-time synchronization between the drive system (1) and the response systems (2). Here, we first give the following feedback controllers that are added on the response system (4) to achieve the fixed-time synchronization:

$$\begin{cases} u_i^R(t) = -\lambda_{1i}^R e_{1i}^R(t-\tau(t)) - \lambda_{1i}^I e_{1i}^I(t-\tau(t)) \\ \qquad -\mathrm{sign}(e_{1i}^R(t))\left[\lambda_{2i} + \lambda_{3i}|e_{1i}^R(t)|^\alpha \right. \\ \qquad \left. +\lambda_{4i}|e_{1i}^R(t)^\beta|\right], \\ u_i^I(t) = -W_{1i}^R e_{1i}^R(t-\tau(t)) - W_{1i}^I e_{1i}^I(t-\tau(t)) \\ \qquad -\mathrm{sign}(e_{1i}^I(t))\left[W_{2i} + \lambda_{3i}|e_{1i}^R(t)|^\alpha \right. \\ \qquad \left. +\lambda_{4i}|e_{1i}^R(t)^\beta|\right], \\ v_j^R(t) = -K_{1j}^R e_{2j}^R(t-\sigma(t)) - K_{1j}^I e_{2j}^I(t-\sigma(t)) \\ \qquad -\mathrm{sign}(e_{2j}^R(t))\left[K_{2j} + K_{3j}|e_{2j}^R(t)|^\alpha \right. \\ \qquad \left. +K_{4j}|e_{2j}^R(t)^\beta|\right], \\ v_j^I(t) = -P_{1j}^R e_{2j}^R(t-\sigma(t)) - P_{1j}^I e_{2j}^I(t-\sigma(t)) \\ \qquad -\mathrm{sign}(e_{2j}^I(t))\left[P_{2j} + K_{3j}|e_{2j}^I(t)|^\alpha \right. \\ \qquad \left. +K_{4j}|e_{2j}^I(t)^\beta|\right], \end{cases} \tag{13}$$

where $i = 1, 2, ..., m$, $j = 1, 2, ..., n$, and constants λ_{1i}^R, λ_{1i}^I, W_{1i}^R, W_{1i}^I, K_{1j}^R, K_{1j}^I, P_{1j}^R, P_{1j}^I, λ_{2i}, W_{2i}, K_{2j}, P_{2j} need to be determined later. Meanwhile λ_{3i}, λ_{4i}, K_{3j}, K_{4j} are any positive constants, $0 < \alpha < 1$, $\beta > 1$.

The symbolic function $\mathrm{sign}(e(t))$ satisfies:

$$\mathrm{sign}(e(t)) = \begin{cases} 1, & e(t) \ge 0, \\ -1, & e(t) < 0. \end{cases}$$

Assumption 5: Let $\lambda = \min\left\{\min\{\lambda_{3i}\}, \min\{K_{3j}\}\right\}$, and $\mu = \min\left\{\min\{\lambda_{4i}\} \cdot m^{\frac{1-\beta}{2}}, \min\{K_{4j}\} \cdot n^{\frac{1-\beta}{2}}\right\}$.

Theorem 1: With Lemma 1-3, if $\lambda_{1i}^R, \lambda_{1i}^I, W_{1i}^R, W_{1i}^I, K_{1j}^R, K_{1j}^I, P_{1j}^R, P_{1j}^I, \lambda_{2i}, W_{2i}, K_{2j}, P_{2j}$ satisfy: $\lambda_{1i}^R \ge \acute{\delta}_i^{R+}$, $\lambda_{1i}^I \ge \acute{\delta}_i^{I+}$, $W_{1i}^R \ge \acute{\delta}_i^{I+}$, $W_{1i}^I \ge \acute{\delta}_i^{R+}$, $K_{1j}^R \ge \acute{\rho}_j^{R+}$, $K_{1j}^I \ge \acute{\rho}_j^{I+}$, $P_{1j}^R \ge \acute{\rho}_j^{I+}$, $P_{1j}^I \ge \acute{\rho}_j^{R+}$, $\lambda_{2i} \ge \chi_i^R$, $W_{2i} \ge \chi_i^I$, $K_{2j} \ge \Omega_i^R$, $P_{2j} \ge \Omega_i^I$, $i = 1, 2, ..., m$, $j = 1, 2, ..., n$, system (1) and system (2) can achieve fixed-time synchronization under the controllers (13). Then the fixed time is $T_{max} = \frac{1}{a(1-p)} + \frac{1}{b(q-1)}$, where constants a, b, p and q are needed to be determined later.

Proof: To prove this theorem, here we choose Lyapunov function as follows:

$$\begin{aligned} V^u(t) =& V_1^R(t) + V_1^I(t) + V_2^R(t) + V_2^I(t) \\ =& V_1^u(t) + V_2^u(t), \end{aligned} \tag{14}$$

where

$$V_1^R(t) = \frac{1}{2}\sum_{i=1}^m (e_{1i}^R(t))^2, \quad V_1^I(t) = \frac{1}{2}\sum_{i=1}^m (e_{1i}^I(t))^2,$$

$$V_2^R(t)=\frac{1}{2}\sum_{j=1}^{n}(e_{2j}^R(t))^2,\ \ V_2^I(t)=\frac{1}{2}\sum_{j=1}^{n}(e_{2j}^I(t))^2,$$
$$V_1^u(t)=V_1^R(t)+V_1^I(t),\ \ V_2^u(t)=V_2^R(t)+V_2^I(t).$$

Remark 2: Here we choose $(e(t))^2$ as the basic term of our Lyapunov function according to our specific model. Comparing with that in [18] where authors chose $|e(t)|$ as the basic term, we do not need to discuss the positive and negative errors separately, which makes it convenient for us to calculate the derivation of the Lyapunov function.

The derivative of $V_1^R(t)$:

$$\begin{aligned}\dot{V}_1^R(t)=&\sum_{i=1}^{m}e_{1i}^R(t)\dot{e}_{1i}^R(t)\\=&\sum_{i=1}^{m}|e_{1i}^R(t)|\mathrm{sign}(e_{1i}^R(t))\Big\{\delta_i^R(\tilde{z}_{1i}^R(t-\tau(t)))\\&\times\tilde{z}_{1i}^R(t-\tau(t))-\delta_i^I(\tilde{z}_{1i}^I(t-\tau(t)))\tilde{z}_{1i}^I(t-\tau(t))\\&+\Big[\delta_i^R(z_{1i}^R(t-\tau(t)))z_{1i}^R(t-\tau(t))\\&-\delta_i^I(z_{1i}^I(t-\tau(t)))z_{1i}^I(t-\tau(t))\Big]\\&+F_i^R(t)+u_i^R(t)\Big\},\\\dot{V}_1^R(t)\le&\sum_{i=1}^{m}\acute{\delta}_i^{R+}|e_{1i}^R(t)||e_{1i}^R(t-\tau(t))|\\&+\acute{\delta}_i^{I+}|e_{1i}^I(t-\tau(t))||e_{1i}^R(t)|\\&+\sum_{i=1}^{m}|e_{1i}^R(t)|\mathrm{sign}(e_{1i}^R(t))\Big\{-\lambda_{1i}^Re_{1i}^R(t-\tau(t))\\&-\lambda_{1i}^Ie_{1i}^I(t-\tau(t))-\mathrm{sign}(e_{1i}^R(t))\cdot\\&\big[\lambda_{2i}+\lambda_{3i}|e_{1i}^R(t)|^{\alpha}+\lambda_{4i}|e_{1i}^R(t)|^{\beta}\big]\Big\}\\&+\sum_{i=1}^{m}|e_{1i}^R(t)||F_i^R(t)|,\end{aligned}$$

with Assumption 1 and Lemma 1, we have:

$$\begin{aligned}\dot{V}_1^R(t)\le&\sum_{i=1}^{m}\Big\{(\acute{\delta}_i^{R+}-\lambda_{1i}^R)|e_{1i}^R(t)||e_{1i}^R(t-\tau(t))|\\&+(\acute{\delta}_i^{I+}-\lambda_{1i}^I)|e_{1i}^R(t)||e_{1i}^I(t-\tau(t))|\Big\}\\&+\sum_{i=1}^{m}(\chi_i^R-\lambda_{2i})|e_{1i}^R(t)|\\&-\sum_{i=1}^{m}\Big[\lambda_{3i}|e_{1i}^R(t)|^{\alpha+1}+\lambda_{4i}|e_{1i}^R(t)|^{\beta+1}\Big]\\\le&-\sum_{i=1}^{m}\Big[\lambda_{3i}|e_{1i}^R(t)|\alpha+1+\lambda_{4i}|e_{1i}^R(t)|^{\beta+1}\Big]\\\le&-\min(\lambda_{3i})\sum_{i=1}^{m}|e_{1i}^R(t)|^{\alpha+1}\\&-\min(\lambda_{4i})\sum_{i=1}^{m}|e_{1i}^R(t)|^{\beta+1}\\\le&-\min(\lambda_{3i})(\sum_{i=1}^{m}|e_{1i}^R(t)|^2)^{\frac{\alpha+1}{2}}\\&-\min(\lambda_{4i})(\sum_{i=1}^{m}|e_{1i}^R(t)|^2)^{\frac{\beta+1}{2}}\cdot m^{\frac{1-\beta}{2}}\\\le&-\min(\lambda_{3i})(V_1^R(t))^{\frac{\alpha+1}{2}}\cdot 2^{\frac{\alpha+1}{2}}\\&-\min(\lambda_{4i})(V_1^R(t))^{\frac{\beta+1}{2}}\cdot m^{\frac{1-\beta}{2}}\cdot 2^{\frac{\beta+1}{2}}.\end{aligned}\tag{15}$$

Proofs of $V_1^I(t)$, $V_2^R(t)$ and $V_2^I(t)$ are similar with that of $V_1^R(t)$.

$$\begin{aligned}\dot{V}_1^I(t)\le&-\min(\lambda_{3i})(V_1^R(t))^{\frac{\alpha+1}{2}}\cdot 2^{\frac{\alpha+1}{2}}\\&-\min(\lambda_{4i})(V_1^R(t))^{\frac{\beta+1}{2}}\cdot m^{\frac{1-\beta}{2}}\cdot 2^{\frac{\beta+1}{2}},\\\dot{V}_2^R(t)\le&-\min(K_{3j})(V_2^R(t))^{\frac{\alpha+1}{2}}\cdot 2^{\frac{\alpha+1}{2}}\\&-\min(K_{4j})(V_1^R(t))^{\frac{\beta+1}{2}}\cdot n^{\frac{1-\beta}{2}}\cdot 2^{\frac{\beta+1}{2}},\\\dot{V}_2^I(t)\le&-\min(K_{3j})(V_2^I(t))^{\frac{\alpha+1}{2}}\cdot 2^{\frac{\alpha+1}{2}}\\&-\min(K_{4j})(V_1^I(t))^{\frac{\beta+1}{2}}\cdot n^{\frac{1-\beta}{2}}\cdot 2^{\frac{\beta+1}{2}}.\end{aligned}\tag{16}$$

According to (14), we have:

$$\begin{aligned}V^u(t)=&V_1^u(t)+V_2^u(t)\\=&\frac{1}{2}\sum_{i=1}^{m}[(e_{1i}^R(t))^2+(e_{1i}^I(t))^2]\\&+\frac{1}{2}\sum_{j=1}^{n}[(e_{2j}^R(t))^2+(e_{2j}^I(t))^2],\\\dot{V}^u(t)\le&-\big\{\min(\lambda_{3i})(V_1^R(t))^{\frac{\alpha+1}{2}}+\min(\lambda_{3i})(V_1^I(t))^{\frac{\alpha+1}{2}}\\&+\min(K_{3j})(V_2^R(t))^{\frac{\alpha+1}{2}}+\min(K_{3j})(V_2^I(t))^{\frac{\alpha+1}{2}}\big\}\\&\cdot 2^{\frac{\alpha+1}{2}}-\big\{\min(\lambda_{4i})(V_1^R(t))^{\frac{\beta+1}{2}}\cdot m^{\frac{1-\beta}{2}}\\&+\min(\lambda_{4i})(V_1^I(t))^{\frac{\beta+1}{2}}\cdot m^{\frac{1-\beta}{2}}\\&+\min(K_{4j})(V_2^R(t))^{\frac{\beta+1}{2}}\cdot n^{\frac{1-\beta}{2}}\\&+\min(K_{4j})(V_2^I(t))^{\frac{\beta+1}{2}}\cdot n^{\frac{1-\beta}{2}}\big\}\cdot 2^{\frac{\beta+1}{2}}\\\le&-\big\{\min(\lambda_{3i})\cdot[V_1^R(t)+V_1^I(t)]^{\frac{\alpha+1}{2}}\\&+\min(K_{3j})\cdot[V_2^R(t)+V_2^I(t)]^{\frac{\alpha+1}{2}}\big\}\cdot 2^{\frac{\alpha+1}{2}}\\&-\big\{\min(\lambda_{4i})\cdot[V_1^R(t)+V_1^I(t)]^{\frac{\beta+1}{2}}\cdot m^{\frac{1-\beta}{2}}\\&+\min(K_{4j})\cdot[V_2^R(t)+V_2^I(t)]^{\frac{\beta+1}{2}}\cdot n^{\frac{1-\beta}{2}}\big\}\cdot 2\\\le&-\lambda[(V_1^u(t))^{\frac{1+\alpha}{2}}+(V_2^u(t))^{\frac{\alpha+1}{2}}]\cdot 2^{\frac{\alpha+1}{2}}\\&-\mu[(V_1^u(t))^{\frac{1+\beta}{2}}+(V_2^u(t))^{\frac{\beta+1}{2}}]\cdot 2\\\le&-\lambda(V^u(t))^{\frac{1+\alpha}{2}}\cdot 2^{\frac{\alpha+1}{2}}-\mu(V^u(t))^{\frac{1+\beta}{2}}\cdot 2^{\frac{3-\beta}{2}}.\end{aligned}\tag{17}$$

According to the results above, they satisfy Lemma 6, so we can conclude that system (1) and system (2) have achieved fixed-time synchronization under our controllers above. Then the synchronization time: $T_{max}=\frac{1}{a(1-p)}+\frac{1}{b(q-1)}$. And $a=\lambda\cdot 2^{\frac{\alpha+1}{2}}$, $p=\frac{\alpha+1}{2}$, $b=\mu\cdot 2^{\frac{3-\beta}{2}}$, $q=\frac{1+\beta}{2}$, where $\lambda=\min\Big\{\min(\lambda_{3i}),\ \min(K_{3j})\Big\}$, $\mu=\min\Big\{\min(\lambda_{4i})\cdot m^{\frac{1-\beta}{2}},\min(K_{4j})\cdot n^{\frac{1-\beta}{2}}\Big\}$.

Remark 3: The feedback controllers (13) consist of several different parts, and every part has its different contribution to achieve synchronization and stability between system (1) and (2). According to our proof above, constants λ_{1i}^R, λ_{1i}^I, W_{1i}^R, W_{1i}^I, K_{1j}^R, K_{1j}^I, P_{1j}^R, P_{1j}^I, λ_{2i}, W_{2i}, K_{2j}, P_{2j} are the main contributors to reach stability of system (1) and (2). Constants λ_{3i}, λ_{4i}, K_{3j}, K_{4j} are the main component to achieve fixed-time synchronization, and the final fixed settling time T_{max} depends on them.

Corollary 1: Based on Lemma 5, we could achieve finite-time synchronization under the following controllers:

$$\begin{cases} u_i^R(t) = -\lambda_{1i}^R e_{1i}^R(t-\tau(t)) - \lambda_{1i}^I e_{1i}^I(t-\tau(t)) \\ \qquad -sign(e_{1i}^R(t))\left[\lambda_{2i}+\lambda_{3i}|e_{1i}^R(t)|^\alpha\right], \\ u_i^I(t) = -W_{1i}^R e_{1i}^R(t-\tau(t)) - W_{1i}^I e_{1i}^I(t-\tau(t)) \\ \qquad -sign(e_{1i}^I(t))\left[W_{2i}+\lambda_{3i}|e_{1i}^R(t)|^\alpha\right], \\ v_j^R(t) = -K_{1j}^R e_{2j}^R(t-\sigma(t)) - K_{1j}^I e_{2j}^I(t-\sigma(t)) \\ \qquad -sign(e_{2j}^R(t))\left[K_{2j}+K_{3j}|e_{2j}^R(t)|^\alpha\right], \\ v_j^I(t) = -P_{1j}^R e_{2j}^R(t-\sigma(t)) - P_{1j}^I e_{2j}^I(t-\sigma(t)) \\ \qquad -sign(e_{2j}^I(t))\left[P_{2j}+K_{3j}|e_{2j}^I(t)|^\alpha\right], \end{cases} \tag{18}$$

where $i = 1, 2, ..., m$, $j = 1, 2, ..., n$, and constants λ_{1i}^R, λ_{1i}^I, W_{1i}^R, W_{1i}^I, K_{1j}^R, K_{1j}^I, P_{1j}^R, P_{1j}^I, λ_{2i}, W_{2i}, K_{2j}, P_{2j} need to be determined later. Meanwhile λ_{3i}, K_{3j}, are any positive constants, $0 < \alpha < 1$. In this paper, in order to simplify our proof and subsequent experiments, we set the same parameters of controller (18) as those of controller (13). Similar to the previous proof of fixed-time synchronization, by constructing the same Lyapunov function, the finite stable maximum time: $T_{max} = \frac{V^{1-p}(0)}{\min\{\min(\lambda_{3i}),\min(K_{3j})\}\cdot 2^{\frac{1+\alpha}{2}}(1-p)}$.

4. ILLUSTRATIVE EXAMPLE

In this section, two examples are shown: Example 1 is to demonstrate the effects of Theorem 1, and Example 2 is an application in chaotic image encryption and decryption based on drive system (1) and response system (2).

Example 1: Considering a two-dimensional memristor-based complex-valued neural network with leakage time-varying delays, we construct our simulation model in this part. The drive system with two-dimension is determined as follows:

$$\begin{aligned} \dot{z}_{1i}^u(t) =& -\delta_i^u(z_{1i}^u(t-\tau(t)))z_{1i}^u(t-\tau(t)) \\ &+\sum_{j=1}^{2} a_{ji}^u(z_{1i}^u(t))f_j^u(z_{2j}^u(t)) \\ &+\sum_{j=1}^{2} b_{ji}^u(z_{1i}^u(t-\tau(t)))f_j^u(z_{2j}^u(t-\sigma(t))), \\ \dot{z}_{2j}^u(t) =& -\rho_j^u(z_{2j}^u(t-\sigma(t)))z_{2j}^u(t-\sigma(t)) \\ &+\sum_{i=1}^{2} c_{ij}^u(z_{2j}^u(t))g_i^u(z_{1i}^u(t)) \\ &+\sum_{i=1}^{2} d_{ij}^u(z_{2j}^u(t-\sigma(t)))g_i^u(z_{1i}^u(t-\tau(t))). \end{aligned} \tag{19}$$

The response system:

$$\begin{aligned} \dot{\tilde{z}}_{1i}^u(t) =& -\delta_i^u(\tilde{z}_{1i}^u(t-\tau(t)))\tilde{z}_{1i}^u(t-\tau(t)) \\ &+\sum_{j=1}^{2} a_{ji}^u(\tilde{z}_{1i}^u(t))f_j^u(\tilde{z}_{2j}^u(t)) \\ &+\sum_{j=1}^{2} b_{ji}^u(\tilde{z}_{1i}^u(t-\tau(t)))f_j^u(\tilde{z}_{2j}^u(t-\sigma(t))) \\ &+u_i^u(t), \\ \dot{\tilde{z}}_{2j}^u(t) =& -\rho_j^u(\tilde{z}_{2j}^u(t-\sigma(t)))\tilde{z}_{2j}^u(t-\sigma(t)) \\ &+\sum_{i=1}^{2} c_{ij}^u(\tilde{z}_{2j}^u(t))g_i^u(\tilde{z}_{1i}^u(t)) \\ &+\sum_{i=1}^{2} d_{ij}^u(\tilde{z}_{2j}^u(t-\sigma(t)))g_i^u(\tilde{z}_{1i}^u(t-\tau(t))) \\ &+v_j^u(t), \end{aligned} \tag{20}$$

$i = 1, 2$, $j = 1, 2$; $T_i = T_j^{'} = 0$, $\Delta_i = \Delta_i^{'} = 1$, $\Lambda_j = \Lambda_j^{'} = 0$, $\delta_i^u = \rho_j^u = 1 + i1$ and $f_j^R(z) = f_j^I(z) = \sin(|z|)$, $g_i^R(z) = g_i^I(z) = \cos(|z|-1)$, $\tau(t) = t + 0.1\sin(t)$, $\sigma(t) = t - 0.1\cos(t)$. The initial values of system (21) are: $\varphi 1^R(s) = (1.5, 2.1)^T$, $\varphi 1^I(s) = (1.35, -1)^T$; $\varphi 2^R(s) = (0.4, 1.25)^T$, $\varphi 2^I(s) = (1, 0.25)^T$. The initial values of system (22) are: $\tilde{\varphi} 1^R(s) = (0.95, -1)^T$, $\tilde{\varphi} 1^I(s) = (1.1, 0.75)^T$, $\tilde{\varphi} 2^R(s) = (0.85, -0.75)^T$, $\tilde{\varphi} 2^I(s) = (-0.6, 1.35)^T$. Meanwhile, the memristor-based connection weights are listed as follows:

$$A^R = \begin{pmatrix} 0.7 & -0.3 \\ 0.5 & 0.1 \end{pmatrix},\ A^{*R} = \begin{pmatrix} -0.5 & 0.2 \\ -0.6 & -1 \end{pmatrix},$$

$$A^I = \begin{pmatrix} -0.8 & 0.5 \\ -0.8 & -1.2 \end{pmatrix},\ A^{*I} = \begin{pmatrix} 0.7 & 0.1 \\ -0.1 & -1.1 \end{pmatrix},$$

$$B^R = \begin{pmatrix} 0.3 & 0.1 \\ 0.7 & -0.6 \end{pmatrix},\ B^{*R} = \begin{pmatrix} 0.4 & 0.2 \\ 0.3 & -0.4 \end{pmatrix},$$

$$B^I = \begin{pmatrix} -0.9 & 0.7 \\ -0.2 & 0.7 \end{pmatrix},\ B^{*I} = \begin{pmatrix} -1.2 & 0.8 \\ -0.4 & 0.9 \end{pmatrix},$$

$$C^R = \begin{pmatrix} -1.5 & 2.5 \\ 0.8 & -1.3 \end{pmatrix},\ C^{*R} = \begin{pmatrix} -1.5 & 2.8 \\ 0.8 & -1.3 \end{pmatrix},$$

$$C^I = \begin{pmatrix} -1.1 & 0.2 \\ 1.1 & -1.3 \end{pmatrix},\ C^{*I} = \begin{pmatrix} -1.3 & 0.5 \\ 1.0 & -1.0 \end{pmatrix},$$

$$D^R = \begin{pmatrix} -1.5 & 0.4 \\ 0.3 & -2 \end{pmatrix},\ D^{*R} = \begin{pmatrix} -1.8 & 0.5 \\ 0.1 & 1.5 \end{pmatrix},$$

$$D^I = \begin{pmatrix} -1.1 & 0.5 \\ 0.4 & -1.5 \end{pmatrix},\ D^{*I} = \begin{pmatrix} -1.2 & 0.6 \\ 0.5 & -1.8 \end{pmatrix}.$$

Some real and imaginary parts of drive system (19) are shown in Figs. 1-4. Errors of drive system (19) and response system (20) without feedback controller is shown

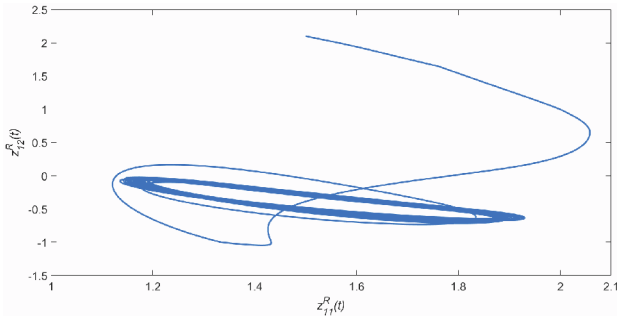

Fig. 1. Phase plot of real part of system (1) with initial conditions $z_{11}^R(0) = 1.5, z_{12}^R(0) = 2.1$.

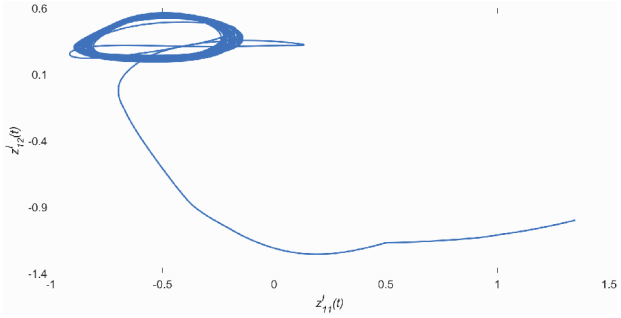

Fig. 2. Phase plot of imaginary part of system (1) with initial conditions $z_{11}^I(0) = 1.35, z_{12}^I(0) = -1$.

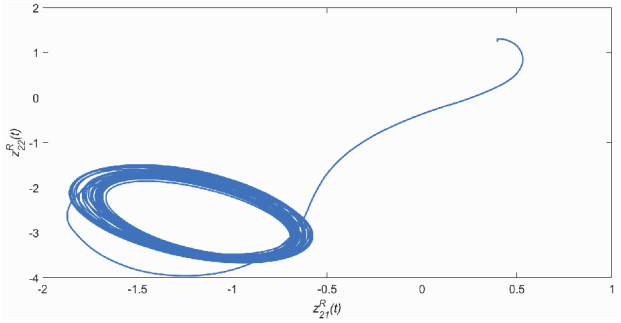

Fig. 3. Phase plot of real part of system (1) with initial conditions $z_{21}^R(0) = 0.4, z_{22}^R(0) = 1.25$.

in Fig. 5. That would be not always equal to zero because the difference of their initial values, if the response system are without controller.

Here, we choose:

$$\lambda_{1i}^R = \lambda_{1i}^I = W_{1i}^R = W_{1i}^I = K_{1j}^R = K_{1j}^I = P_{1j}^R = P_{1j}^I = 1;$$
$$\lambda_{3i} = \lambda_{4i} = 0.4;\ \ k_{3j} = K_{3j} = 0.6;\ \text{for } i = j = 1,2.$$
$$\lambda_{21} = \lambda_{22} = W_{21} = W_{22} = 12;\ \ K_{21} = K_{22} = P_{21} = P_{22} = 20.$$

So our feedback controllers are:

$$\begin{aligned} u_1^R(t) =& -e_{11}^R(t-\tau(t)) - e_{11}^I(t-\tau(t)) \\ & -\text{sign}(e_{11}^R(t))[12+0.4|e_{11}^R(t)|^\alpha + 0.4|e_{11}^R(t)|^\beta], \end{aligned}$$

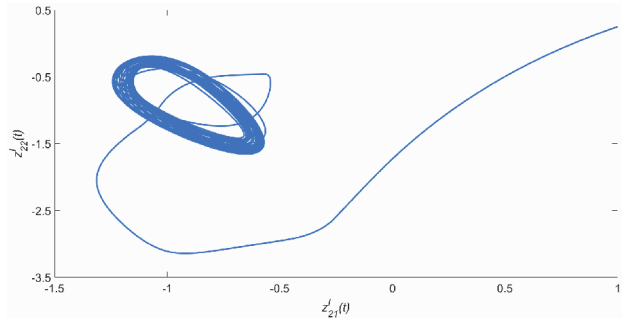

Fig. 4. Phase plot of imaginary Part of system (1) with initial conditions $z_{21}^I(0) = 1, z_{22}^I(0) = 0.25$.

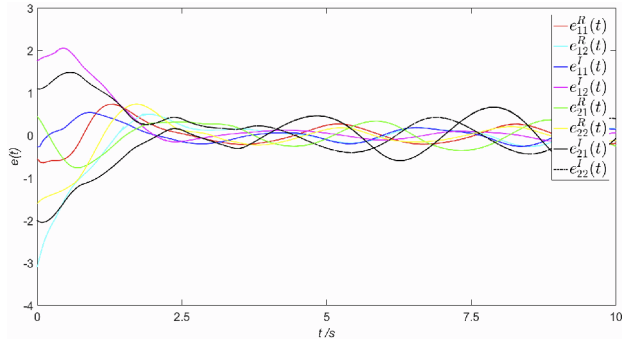

Fig. 5. Synchronization errors without controllers.

$$\begin{aligned} u_1^I(t) =& -e_{11}^R(t-\tau(t)) - e_{11}^I(t-\tau(t)) \\ & -\text{sign}(e_{11}^I(t))[12+0.4|e_{11}^I(t)|^\alpha + 0.4|e_{11}^I(t)|^\beta], \\ u_2^R(t) =& -e_{12}^R(t-\tau(t)) - e_{12}^I(t-\tau(t)) \\ & -\text{sign}(e_{12}^R(t))[12+0.4|e_{12}^R(t)|^\alpha + 0.4|e_{12}^R(t)|^\beta], \\ u_2^I(t) =& -e_{12}^R(t-\tau(t)) - e_{12}^I(t-\tau(t)) \\ & -\text{sign}(e_{12}^I(t))[12+0.4|e_{12}^I(t)|^\alpha + 0.4|e_{12}^I(t)|^\beta], \\ v_1^R(t) =& -e_{21}^R(t-\tau(t)) - e_{21}^I(t-\rho(t)) \\ & -\text{sign}(e_{21}^R(t))[20+0.6|e_{21}^R(t)|^\alpha + 0.6|e_{21}^R(t)|^\beta], \\ v_1^I(t) =& -e_{21}^R(t-\tau(t)) - e_{21}^I(t-\rho(t)) \\ & -\text{sign}(e_{21}^I(t))[20+0.6|e_{21}^I(t)|^\alpha + 0.6|e_{21}^I(t)|^\beta], \\ v_2^R(t) =& -e_{22}^R(t-\tau(t)) - e_{22}^I(t-\rho(t)) \\ & -\text{sign}(e_{22}^R(t))[20+0.6|e_{22}^R(t)|^\alpha + 0.6|e_{22}^R(t)|^\beta], \\ v_2^I(t) =& -e_{22}^R(t-\tau(t)) - e_{22}^I(t-\rho(t)) \\ & -\text{sign}(e_{22}^I(t))[20+0.6|e_{22}^I(t)|^\alpha + 0.6|e_{22}^I(t)|^\beta]. \end{aligned} \tag{21}$$

Remark 4: System (19) and (20) can achieve fixed-time synchronization under the controllers (21) with appropriate parameters according to Theorem 1. Obviously, all the parameters follow these detailed inequalities as follows: $\lambda_{1i}^R \geq \acute{\delta}_i^{R+} = 1$, $\lambda_{1i}^I \geq \acute{\delta}_i^{I+} = 1$, $W_{1i}^R \geq \acute{\delta}_i^{I+} = 1$, $W_{1i}^I \geq \acute{\delta}_i^{R+} = 1$, $K_{1j}^R \geq \acute{\rho}_j^{R+} = 1$, $K_{1j}^I \geq \acute{\rho}_j^{I+} = 1$, $P_{1j}^R \geq \acute{\rho}_j^{I+} = 1$, $P_{1j}^I \geq \acute{\rho}_j^{R+} = 1$, for $i = j = 1, 2$. $\lambda_{21} \geq \chi_1^R = 11.2$, $W_{21} \geq$

$\chi_1^I = 11.2$, $\lambda_{22} \geq \chi_2^R = 11$, $W_{22} \geq \chi_2^I = 11$, $K_{21} \geq \Omega_1^R = 18.4$, $P_{21} \geq \Omega_1^I = 18.4$, $K_{22} \geq \Omega_2^R = 18$, $P_{22} \geq \Omega_2^I = 18$.

Remark 5: In the controllers above or in (13), (18), etc., discontinuous signum function may be unsuitable in practical applications and signum function can produce the undesired chattering [28], which degrades the performance. So we choose function $e(t)/(e(t)+\delta)$ to replace the symbolic function, where δ is sufficiently small. In this way, we can weaken this chattering.

Instead, with Theorem 1, we know that the fixed-time synchronization $T_{max} = 11.89$ under our own controllers. The result of synchronization errors is shown in Fig. 8, and some parts of the state trajectories are shown in Figs. 6-7 and Figs. 9-10. In our simulation, the fixed stable time $T(e_0) = 0.26$, when $V(T(e_0)) \equiv 0$, and obviously, $T(e_0) \leq T_{max}$. So it can definitely demonstrate the effectiveness of the results in Theorem 1.

According to Corollary 1, we achieve finite-time synchronization under our feedback controllers as follows:

$$\begin{aligned} u_1^R(t) =& -e_{11}^R(t-\tau(t)) - e_{11}^I(t-\tau(t)) \\ & - \text{sign}(e_{11}^R(t))[12+0.4|e_{11}^R(t)|^\alpha], \\ u_1^I(t) =& -e_{11}^R(t-\tau(t)) - e_{11}^I(t-\tau(t)) \\ & - \text{sign}(e_{11}^I(t))[12+0.4|e_{11}^I(t)|^\alpha], \end{aligned}$$

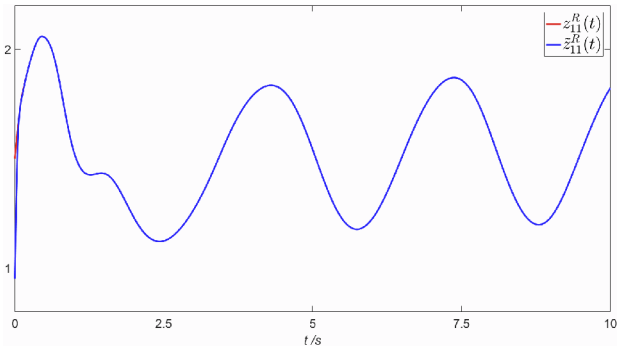

Fig. 6. The state trajectories of z_{11}^R, $\tilde{z}_{11}^R$ with initial conditions $z_{11}^R(0) = 1.5$, $\tilde{z}_{11}^R(0) = 0.95$.

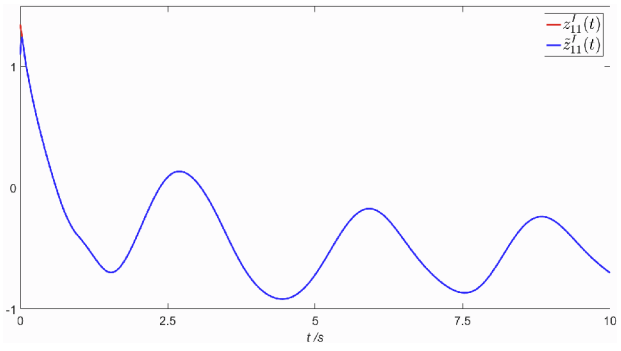

Fig. 7. The state trajectories of z_{11}^I, $\tilde{z}_{11}^I$ with initial conditions $z_{11}^I(0) = 1.35$, $\tilde{z}_{11}^I(0) = 1.1$.

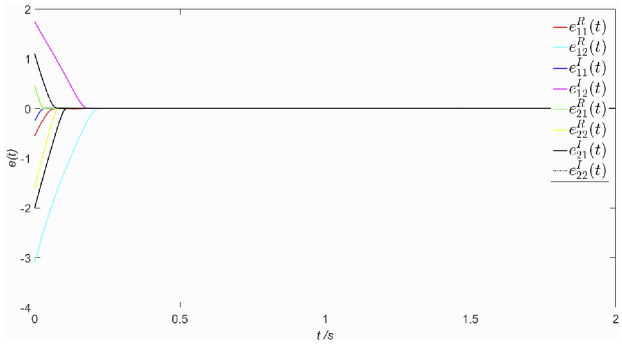

Fig. 8. Synchronization errors with controllers.

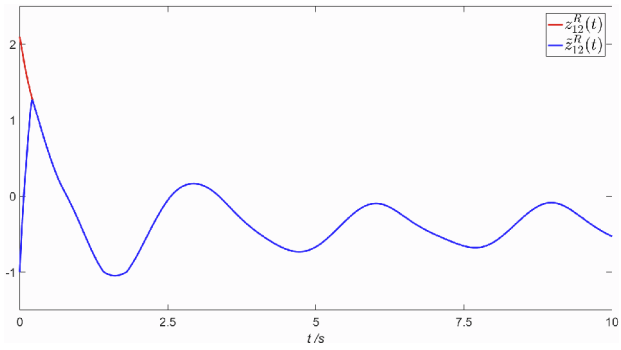

Fig. 9. The state trajectories of z_{12}^R, $\tilde{z}_{12}^R$ with initial conditions $z_{12}^R(0) = 2.1$, $\tilde{z}_{12}^R(0) = -1$.

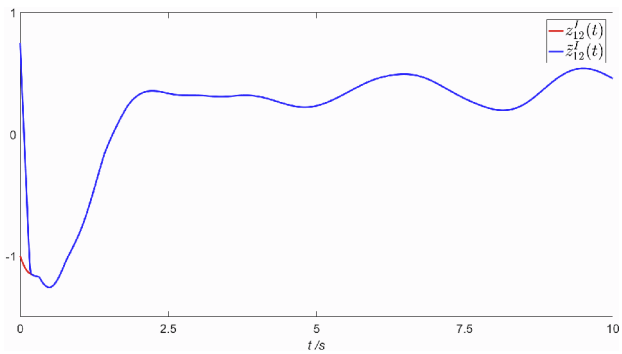

Fig. 10. The state trajectories of z_{12}^I, $\tilde{z}_{12}^I$ with initial conditions $z_{12}^I(0) = -1$, $\tilde{z}_{12}^I(0) = 0.75$.

$$\begin{aligned} u_2^R(t) =& -e_{12}^R(t-\tau(t)) - e_{12}^I(t-\tau(t)) \\ & - \text{sign}(e_{12}^R(t))[12+0.4|e_{12}^R(t)|^\alpha], \\ u_2^I(t) =& -e_{12}^R(t-\tau(t)) - e_{12}^I(t-\tau(t)) \\ & - \text{sign}(e_{12}^I(t))[12+0.4|e_{12}^I(t)|^\alpha], \\ v_1^R(t) =& -e_{21}^R(t-\tau(t)) - e_{21}^I(t-\rho(t)) \\ & - \text{sign}(e_{21}^R(t))[20+0.6|e_{21}^R(t)|^\alpha], \\ v_1^I(t) =& -e_{21}^R(t-\tau(t)) - e_{21}^I(t-\rho(t)) \\ & - \text{sign}(e_{21}^I(t))[20+0.6|e_{21}^I(t)|^\alpha], \\ v_2^R(t) =& -e_{22}^R(t-\tau(t)) - e_{22}^I(t-\rho(t)) \end{aligned}$$

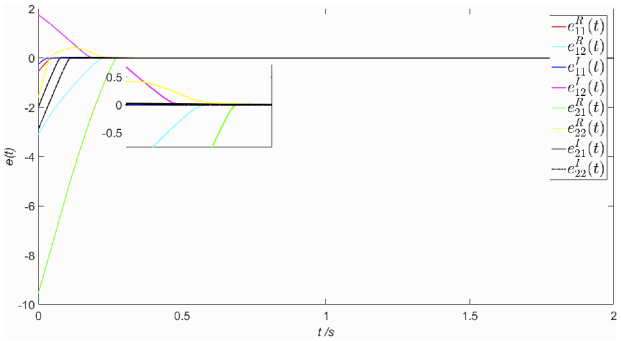

Fig. 11. Finite-time synchronization errors with the new initial values.

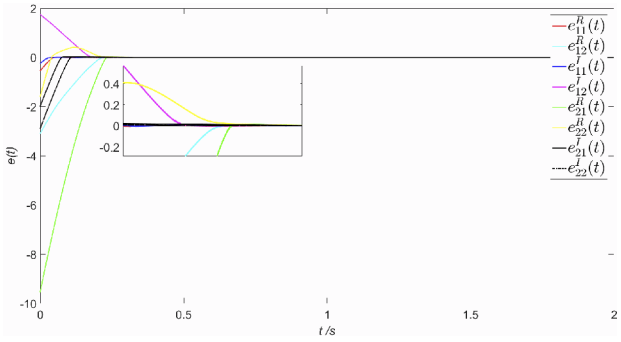

Fig. 12. Fixed-time synchronization errors with the new initial values.

$$
\begin{aligned}
&-\operatorname{sign}(e_{22}^{R}(t))[20+0.6|e_{22}^{R}(t)|^{\alpha}],\\
v_2^{I}(t) = &-e_{22}^{R}(t-\tau(t))-e_{22}^{I}(t-\rho(t))\\
&-\operatorname{sign}(e_{22}^{I}(t))[20+0.6|e_{22}^{I}(t)|^{\alpha}]. \qquad (22)
\end{aligned}
$$

To distinguish the difference between finite-time and fixed-time synchronization better, here we enlarge the initial synchronization errors. The new initial values of neurons are: $\varphi 1^{R}(s) = (1.5,2.1)^{T}$; $\varphi 1^{I}(s) = (1.35,-1)^{T}$; $\varphi 2^{R}(s) = (10.4,1.25)^{T}$; $\varphi 2^{I}(s) = (1,4.25)^{T}$; $\widetilde{\varphi} 1^{R}(s) = (0.95,-1)^{T}$; $\widetilde{\varphi} 1^{I}(s) = (1.1,0.75)^{T}$; $\widetilde{\varphi} 2^{R}(s) = (0.85,-0.75)^{T}$; $\widetilde{\varphi} 2^{I}(s) = (-0.6,1.35)^{T}$. The finite-time synchronization errors are shown in Fig. 11, and the fixed-time synchronization errors are shown in Fig. 12 with the same new initial values above. According to Theorem 1, we can calculate that the finite-time synchronization $T_{max} = 22.98$ under controllers (22), and the fixed-time synchronization $T_{max} = 11.89$ under controllers (21) according to Corollary 1. With the new initial values, the curve of controllers (21)(22) are shown in Figs. 13 and 14.

Remark 6: In simulation, with the new initial values, the fixed stable time $T(e_O) = 0.60$, while $T(e_O) = 0.26$ with old initial values in our first simulation. So the stable time $T(e_0)$ can change with the initial values, but T_{max} would not change no matter what the initial errors are. In

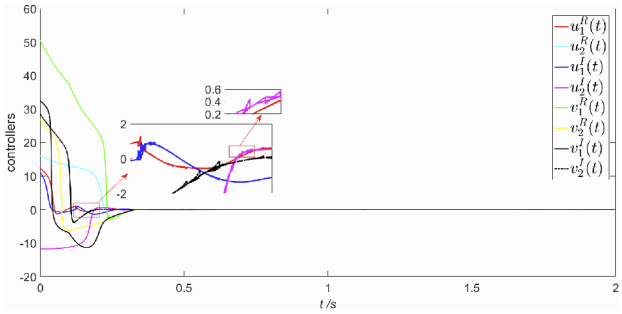

Fig. 13. The curve of controller (21) with the new initial values.

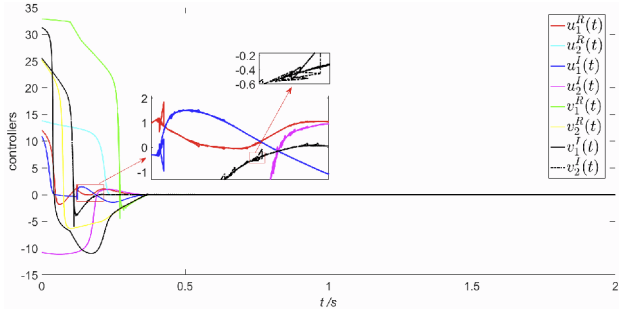

Fig. 14. The curve of controller (22) with the new initial values.

result, the fixed-time synchronization maximum time T_{max} with new initial values is equal to the previous one.

Example 2: Here we use the chaotic characters of drive system (19) and response system (20) to achieve applications in image encryption and decryption. In this example, we define the initial values of system (21) are: $\varphi 1^{R}(s) = (1.5,2.1)^{T}$; $\varphi 1^{I}(s) = (1.35,-1)^{T}$; $\varphi 2^{R}(s) = (0.4,1.25)^{T}$; $\varphi 2^{I}(s) = (3.6,4.25)^{T}$; The initial values of response system (22) are: $\widetilde{\varphi} 1^{R}(s) = (0.95,-1)^{T}$; $\widetilde{\varphi} 1^{I}(s) = (1.1,0.75)^{T}$; $\widetilde{\varphi} 2^{R}(s) = (0.85,-0.75)^{T}$; $\widetilde{\varphi} 2^{I}(s) = (-0.6,1.35)^{T}$.

According to the drive system (19), our encryption algorithm is designed as follows:

Step 1: We choose the classical picture "Lena", and its size is $M \times N$ in RGB, $M = 256$, $N = 256$.

Step 2: According to our drive system (19), we can get the sequence of $z_{11(k_1)}^{R} = [z_{11(1)}^{R}, z_{11(2)}^{R}, \ldots, z_{11(256\cdot128)}^{R}]$, and $z_{11(k_2)}^{I} = [z_{11(1)}^{I}, z_{11(2)}^{I}, \ldots, z_{11(256\cdot128)}^{I}]$. $\delta 1 = sort(round(z_{11(k_1)}^{R}, -3))$ and $\delta 2 = sort(round(z_{11(k_2)}^{I}, -3))$. $\delta 1$ is used to reorder one half of this picture, and $\delta 2$ is used to reorder another half of this picture:

$$
\begin{aligned}
&R(i) = R(\delta 1(i)); \quad G(i) = G(\delta 1(i)); \quad B(i) = B(\delta 1(i));\\
&R(i+\text{length}/2) = R(\delta 2(i)+\text{length}/2);\\
&G(i+\text{length}/2) = G(\delta 2(i)+\text{length}/2);\\
&B(i+\text{length}/2) = B(\delta 2(i)+\text{length}/2);
\end{aligned}
$$

$$NR = reshape(R,M,N);\ \ NG = reshape(G,M,N);$$
$$NB = reshape(B,M,N);\ \text{for } i = 1,2,...,\text{length}/2. \tag{23}$$

Step 3: The real part sequences of the left three neurons of system (19) encrypt the even point of picture, and the imaginary part sequences encrypt the odd point of this picture:

$$\begin{aligned}
&z1(k) = z^R_{12(k)},\ z2(k) = z^I_{12(k)},\ \text{for } k = 1,2,...,256\times 256;\\
&\text{if}\quad \text{mod}\,(i,2) == 0\\
&\qquad z11(i,j) = 1e15 * (z1(k) - floor(z1(k)));\\
&\qquad z11(i,j) = floor(mod(z11(i,j),256));\\
&\qquad newR(i,j) = bitxor(z11(i,j),NR(i,j));\\
&\text{else}\\
&\qquad z22(i,j) = 1e15 * (z2(k) - floor(z1(k)));\\
&\qquad z22(i,j) = floor(mod(z22(i,j),256));\\
&\qquad newR(i,j) = bitxor(z22(i,j),NR(i,j)).
\end{aligned} \tag{24}$$

According to CVMBAMNN and fixed-time synchronization between drive and response system, the flow chart of image encryption and decryption is shown in Fig. 17. With our encryption algorithm, the result of encryption is shown in Fig. 16, while its original picture is shown in Fig. 15. From the histograms of original picture and encrypted picture shown in Fig. 18-19, it can be said that image becomes highly unordered after encryption. The correlation coefficient of R for original and encrypted pictures is shown in Figs. 20-21 respectively. After encryption, the image correlation coefficient become much lower.

Based on fixed-time synchronization between drive system (19) and response system (20), the decryption algorithm is the contrary method of encryption algorithm, and the decrypted picture is shown in Fig. 23. Besides, because its susceptibility of initial values, when the initial value of any one of these neurons change, it would be not decrypted successfully. Here we give the false decrypted picture shown in Fig. 22 with $z^R_{11}(0) = 1.5 + 10^{-13}$.

Based on our image encryption algorithm, horizontal correlation coefficient of R channel for encrypted "Lena" is shown in Table 1. Tables 2 and 3 list the comparative analysis of average value of correlation coefficient and information entropy obtained from our algorithm with oth-

Fig. 15. Original picture "Lena".

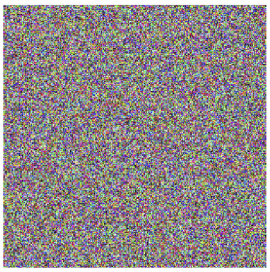

Fig. 16. The encrypted picture.

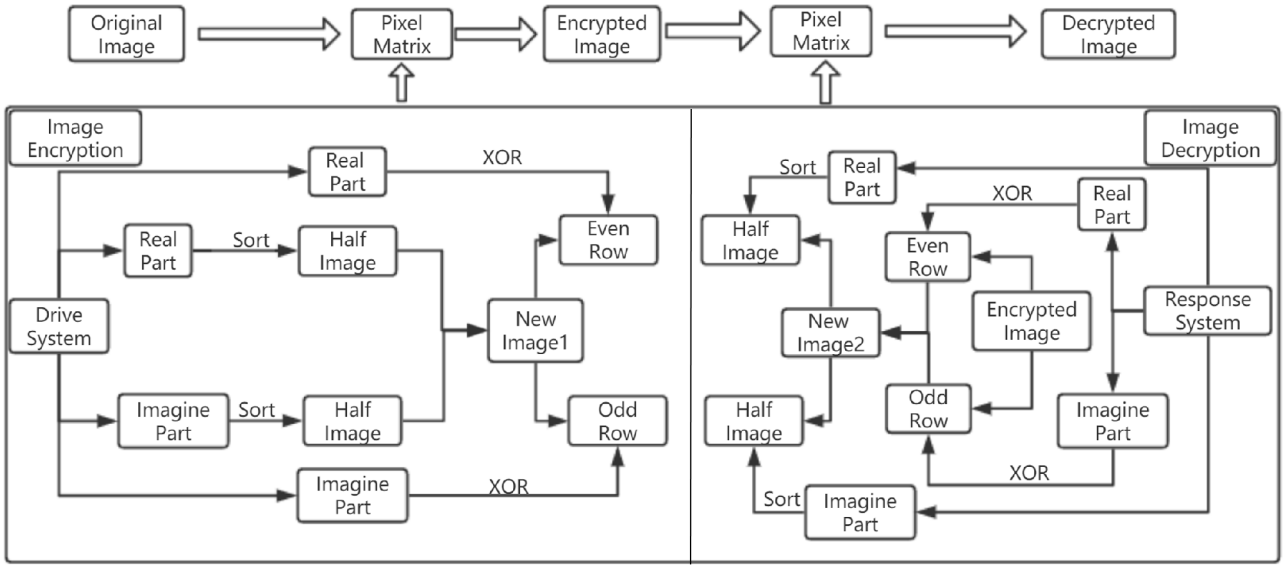

Fig. 17. Flow chart of encryption and decryption algorithm.

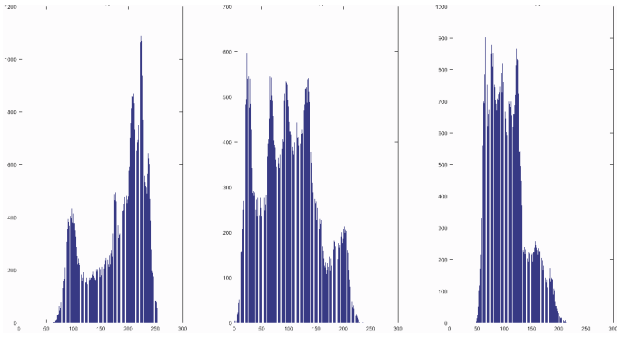

Fig. 18. Histograms of RGB for original picture.

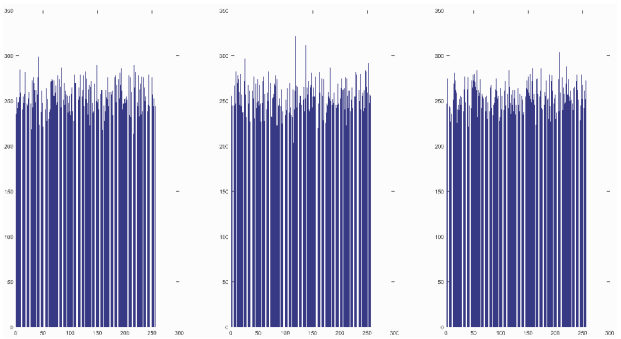

Fig. 19. Histograms of RGB for encrypted picture.

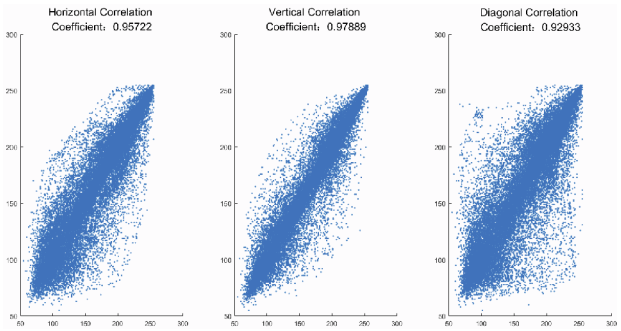

Fig. 20. Horizontal, vertical and diagonal correlation coefficient of R for original picture.

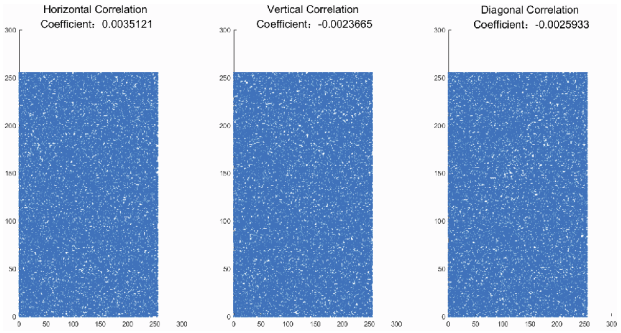

Fig. 21. Horizontal, vertical and diagonal correlation coefficient of R for encrypted picture.

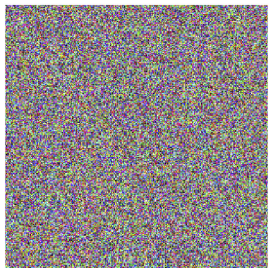

Fig. 22. The false decrypted picture when the initial value of $z_{11}^{R}(0) = 1.5 + 10^{-13}$.

Fig. 23. The right decrypted picture.

Table 1. Horizontal correlation coefficient.

	R	G	B
Original Lena	0.9572	0.9432	0.9284
Encrypted Lena	0.0035	0.0011	0.0021

Table 2. Comparison of correlation coefficients of encrypted "Lena" (average value of the color channels).

	Horizontal	Vertical	Diagonal
Our algorithm	**0.0022**	**-0.0004**	**-0.0007**
[29]	0.0038	0.0041	0.0036
[30]	0.0445	-0.0186	-0.0022
[31]	0.0816	0.0401	0.0047
[32]	0.0075	0.0128	0.0049

Table 3. Information entropy results.

	R	G	B
Our algorithm	7.9972	**7.9974**	**7.9976**
[29]	**7.9976**	7.9971	7.9968
[30]	7.9278	7.9744	7.9705
[33]	7.9901	7.9898	7.9896

ers, respectively. Obviously, most results of our algorithm are much better than those of the previous others, especially in average correlation coefficient.

5. CONCLUSION

In this paper, we construct the model of CVMBAM neural network with leakage time-varying delays, which little work has been studied before. By analyzing the dynamic characteristics of CVMBAM neural network, we have observed that such neural network inherits the hyper chaotic character of BAM neural network. Besides, to ensure the efficiency, rapidity and stability of image transmission, we design feedback controllers to achieve fixed-time and finite-time synchronization with comparative analysis experiment. In the end, the effectiveness of our results is validated by numerical examples, and applications in chaotic image encryption and decryption are shown above. Due to high consistence of our system, corresponding initial values of decryption are highly sensitive. In future research, we will study with the case where leakage time-varying delays and the bound of the rates of neuron self-inhibition are unknown, which may better improve the neurodynamic model.

REFERENCES

[1] B. Kosko, "Bidirectional associative memories," *Systems Man & Cybernetics IEEE Transactions on*, vol. 18, no. 1, pp. 49-60, 1988.

[2] B. Fa, Y. Yin, and C. Fu, "The bidirectional associative memory neural network based on fault tree and its application to inverter's fault diagnosis," *Proc. of IEEE International Conference on Intelligent Computing and Intelligent Systems, ICIS 2009*, vol. 1, pp. 209-213, 2009.

[3] G. Mathai and B. R. Upadhyaya, "Performance analysis and application of the bidirectional associative memory to industrial spectral signatures," *International Joint Conference on Neural Networks*, IEEE, vol. 1, pp. 33-37, 1989.

[4] W. P. Wang, M. H. Yu, X. Luo, L. L. Liu, M. M. Yuan, and W. B. Zhao, "Synchronization of memristive BAM neural networks with leakage delay and additive time-varying delay components via sampled-data control," *Chaos, Solitons & Fractals*, vol. 104, pp. 84-97, 2017.

[5] D. Liu, S. Zhu, and E. Ye, "Synchronization stability of memristor-based complex-valued neural networks with time delays," *Neural Networks*, vol. 96, pp. 115-127, 2017.

[6] J. M. Zurada, I. Aizenberg, and M. A. Mazurowski, "Learning in networks: complex-valued neurons, pruning, and rule extraction," *Proc. of the 4th International IEEE Conference on Intelligent Systems, IS'08*, vol. 1, pp. 1-15-1-20, 2008.

[7] J. Rubio, "Stable Kalman filter and neural network for the chaotic systems identification," *Journal of the Franklin Institute*, vol. 354, no. 16, pp. 7444-7462, 2017.

[8] E. Lughofer, S. Kindermann, M. Pratama, and J. Rubio, "Top-down sparse fuzzy regression modeling from data with improved coverage," *International Journal of Fuzzy Systems*, vol. 19, no. 5, pp. 1645-1658, 2017.

[9] J. Rubio, E. Lughofer, J. A. Meda-Campaña, L. A. Páramo, J. F. Novoa, and J. Pacheco, "Neural network updating via argument Kalman filter for modeling of Takagi-Sugeno fuzzy models," *Journal of Intelligent, Fuzzy Systems*, vol. 35, no. 2, pp. 2585-2596, 2018.

[10] J. Rubio, E. Lughofer, A. Plamen, J. F. Novoa, and J. A. Meda-Campaña, "A novel algorithm for the modeling of complex processes," *Kybernetika*, vol. 54, no. 1, pp. 79-95, 2018.

[11] M. Kar, M. K. Mandal, and D. Nandi, "RGB image encryption using hyper chaotic system," *Research in Computational Intelligence and Communication Networks (ICRCICN), 2017 Third International Conference on. IEEE*, pp. 354-359, 2017.

[12] H. Liu, Z. Wang, B. Shen, and X. Liu, "Event-triggered $H\infty$ state estimation for delayed stochastic memristive neural networks with missing measurements: the discrete time case," *IEEE Transactions on Neural Networks and Learning Systems*, vol. 29, no. 8, pp. 3726-3737, 2017.

[13] X. Li, X. Fu, P. Balasubramaniam, and R. Rakkiyappan, "Existence, uniqueness and stability analysis of recurrent neural networks with time delay in the leakage term under impulsive perturbations," *Nonlinear Analysis: Real World Applications*, vol. 11, no. 5, pp. 4092-4108, 2010.

[14] Z. S. Wang, J. Sun, and H. G. Zhang, "Stability analysis of T-S fuzzy control system with sampled-dropouts based on time-varying Lyapunov function method," *IEEE Transactions on Systems, Man, and Cybernetics: Systems (Early Access)*, pp. 1-12, 2018.

[15] G. Velmurugan, R. Rakkiyappan, and J. Cao, "Finite-time synchronization of fractional-order memristor-based neural networks with time delays," *Neural Networks the Official Journal of the International Neural Network Society*, vol. 73, no. 1-2, pp. 36-46, 2015.

[16] J. Mei, M. H. Jiang, W. M. Xu, and B. Wang, "Finite-time synchronization control of complex dynamical networks with time delay," *Communications in Nonlinear Science & Numerical Simulation*, vol. 18, no. 9, pp. 2462-2478, 2013.

[17] X. Yang, J. Lam, and D. W. C. Ho, "Fixed-time synchronization of complex networks with impulsive effects via nonchattering control," *IEEE Transactions on Automatic Control*, vol. 62, no. 11, pp. 5511-5521, 2017.

[18] Y. Wan, J. Cao, G. Wen, and W. Yu, "Robust fixed-time synchronization of delayed Cohen-Grossberg neural networks," *Neural Networks*, vol. 73, pp. 86-94, 2016.

[19] A. Polyakov, "Nonlinear feedback design for fixed-time stabilization of linear control systems," *IEEE Transactions on Automatic Control*, vol. 57, no. 8, pp. 2106-2110, 2012.

[20] L. Sui, K. Duan, J. Liang, and X. Hei, "Asymmetric double-image encryption based on cascaded discrete fractional random transform and logistic maps," *Optics Express*, vol. 22, no. 9, pp. 10605-10621, 2014.

[21] S. Liu and F. Zhang, "Complex function projective synchronization of complex chaotic system and its applications in secure communication," *Nonlinear Dynamics*, vol. 76, no. 2, pp. 1087-1097, 2014.

[22] R. Matthews, "On the derivation of a "chaotic" encryption algorithm," *Cryptologia*, vol. 8, no. 8, pp. 29-41, 1989.

[23] C. Fu, Y. Zheng, M. Chen, and Z. K. Wen, "A color image encryption algorithm using a new 1-D chaotic map," *Proc. of IEEE 17th International Conference on Communication Technology (ICCT)*, IEEE, pp. 1768-1773, 2018.

[24] H. C. Li, T. P. Zhang, and Z. M. Guo, "Adaptive control for a class of uncertain chaotic systems with saturation nonlinear input," *Proc. of the 9th International Conference on Electronic Measurement, Instruments*, pp. 3-583-3-587, 2009.

[25] J. Chen, J. Ping, and Z. Zeng, "Global Mittag-Leffler stability and synchronization of memristor-based fractional-order neural networks," *Neural Networks*, vol. 51, no. 3, pp. 1-8, 2014.

[26] G. Hardy, J. E. Littlewood, and G. Polya, *Inequalities*, Cambridge Univ Press, Cambridge, 1952.

[27] X. Liu, W. Lu, and T. Chen, "Finite-time and fixed-time stability and synchronization," *Proc. of Control Conference IEEE*, pp. 7985-7989, 2016.

[28] J. H. Wang, W. S. Luo, and L. G. Wu, "Adaptive type-2 FNN-based dynamic sliding mode control of DC-DC boost converters," *IEEE Transactions on Systems, Man, and Cybernetics: Systems (Early Access)*, pp. 1-12, 2019.

[29] M. Kar, M. K. Mandal, and D. Nandi, "RGB image encryption using hyper chaotic system," *Proc. of the 3rd International Conference on Research in Computational Intelligence and Communication Networks (ICRCICN)*, pp. 354-359, 2017.

[30] A. Kadira, A. Hamdullaa, and W. Q. Guo, "Color image encryption using skew tent map and hyper chaotic system of 6th-order CNN," *Optik*, vol. 125 pp. 1671-1675, 2014.

[31] L. Zhang, X. Liao, and X. Wang, "An image encryption approach based on chaotic maps," *Chaos, Solitons & Fractals*, vol. 24, pp. 759-765, 2005.

[32] S. Mazloom and A. M. Eftekhari-Moghadam, "Colour image encryption based on coupled nonlinear chaotic map," *Chaos, Solitons & Fractals*, vol. 42, pp. 1745-1754, 2009.

[33] X. P. Wei, L. Guo, Q. Zhang, J. Zhang, and S. Lian, "A novel color image encryption algorithm based on DNA sequence operation and hyper-chaotic system," *J. Syst. Software*, vol. 85, pp. 290-299, 2012.

Yongzhen Guo received his master degree of Control Theory and Control Engineering from Tianjin University, Tianjin, China. He is studying for a Ph.D. at the School of Automation,Beijing Institute of Technology (BIT). He is also the General Manager of Industrial Control System Evaluation and Certification Department of China Software Testing Center. He received National Science and Technology Major Projects, and National Key Research and Development Programs. His research area is security and cryptography, safety and reliability, and system evaluation and certification. As a member of SAC/TC124/SC10, SAC/TC196, ISO/TC 199/WG8, IEC/TC65/SC 65C/WG18, he is participating in a number of international standards and national standards setting and revising.

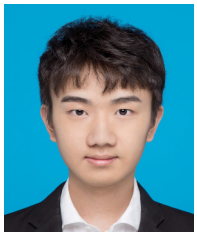

Yang Luo is currently pursuing a bachelor's degree in intelligent science and technology from University of Science and Technology Beijing, Beijing, China. His current research interests include memristive neural networks, system control and chaotic image encryption and decryption.

Weiping Wang received her Ph.D. degree in telecommunications physics electronics from Beijing University of Posts and Telecommunications, Beijing, China, in 2015. She is currently an Associate Professor with the Department of Computer and Communication Engineering, University of Science and Technology Beijing. She received the the National Key Research and Development Program of China, the State Scholarship Fund of China Scholarship Council, National Natural Science Foundation of China, the Postdoctoral fund, and the basic scientific research project. Her current research interests include brain-like computing, memrisitive neural network, associative memory awareness simulation, complex network, network security and image encryption.

Xiong Luo received his Ph.D. degree in computer applied technology from Central South University, Changsha, China, in 2004. He is currently a Professor with the School of Computer and Communication Engineering, University of Science and Technology Beijing, Beijing, China. His current research interests include neural networks, machine learning, and computational intelligence. He has published extensively in his areas of interest in several journals, such as IEEE ACCESS, Future Generation Computer Systems, and Personal and Ubiquitous Computing.

Chao Ge received his Ph.D. degree in electrical engineering from Yanshan University, Qinhuangdao, China, in 2015. Now he is an Associate Professor in North China University of Science and Technology, China. His research interests are in time-delay systems, neural networks, fuzzy systems and networked control systems.

Jürgen Kurths studied mathematics at the University of Rostock and received his Ph.D. degree in 1983 from the GDR Academy of Sciences. He was a full professor at the University of Potsdam from 1994 to 2008 and has been a professor of nonlinear dynamics at the Humboldt University, Berlin, and the chair of the research domain Transdisciplinary Concepts of the Potsdam Institute for Climate Impact Research since 2008 and a sixth-century chair of Aberdeen University, United Kingdom, since 2009. He is a fellow of the American Physical Society. He received the Alexander von Humboldt Research Award from CSIR, India, in 2005 and an honorary doctorate in 2008 from the Lobachevsky University Nizhny Novgorod and one in 2012 from the State University Saratov. He became a member of the Academia Europaea in 2010 and of the Macedonian Academy of Sciences and Arts in 2012. His primary research interests include synchronization, complex networks, and time series analysis and their applications. He has published more than 500 papers that are cited more than 18,000 times (H-factor: 57). He is an editor of journals such as PLoS ONE, the Philosophical Transaction of the Royal Society A, the Journal of Nonlinear Science, and Chaos.

Manman Yuan received her M.S. degree in computer science and technology from Inner Mongolia University of Science and Technology, Baotou, China, in 2015, where she is currently pursuing a Ph.D. degree from University of Science and Technology Beijing, Beijing, China. Her current research interests include memristive neural networks and brain computing.

Yang Gao is an assistant research fellow with the China Information Technology Security Evaluation Center. She received her M.S. degree in applied mathematics and her Ph.D. degree in information security from Beijing University of Posts and Telecommunications, China. Her current research interests include information security, complex networks, cyber-physical system, ICS security.